

## ***NIST Technical Note 1420***

---

# ***NIST High-Accuracy Sampling Wattmeter***

---

Gerard N. Stenbakken

Amos Dolev

Electricity Division  
Electronics and Electrical Engineering Laboratory  
National Institute of Standards and Technology  
Gaithersburg, MD 20899-0001

9-88016-1  
11/1/96

August 1996



**U.S. Department of Commerce**

Michael Kantor, Secretary

**Technology Administration**

Mary L. Good, Under Secretary for Technology

**National Institute of Standards and Technology**

Arati Prabhakar, Director

---

National Institute of Standards  
and Technology  
Technical Note 1420  
Natl. Inst. Stand. Technol.  
Tech. Note 1420  
54 pages (Aug. 1996)  
CODEN: NTNOEF

U.S. Government Printing Office  
Washington: 1996

For sale by the Superintendent of  
Documents  
U.S. Government Printing Office  
Washington, DC 20402

## Table of Contents

	page
List of Figures . . . . .	v
List of Tables . . . . .	v
Abstract . . . . .	1
1. Introduction . . . . .	1
2. System Operation . . . . .	2
2.1. Power Sampling Basics . . . . .	2
2.2. General Operation . . . . .	3
3. Hardware Changes . . . . .	3
3.1. Amplifier and Conversion Modules . . . . .	4
3.1.1. Voltage Inputs . . . . .	4
3.1.1.1. The Attenuator . . . . .	5
3.1.1.2. Instrumentation Amplifier . . . . .	5
3.1.1.3. A/D Converter Cards . . . . .	6
3.1.2. Current Inputs . . . . .	7
3.1.2.1. Two-Stage Input Transformer . . . . .	8
3.1.2.2. I/V Card . . . . .	10
3.1.3. Clock-Synchronizer Card . . . . .	12
3.1.4. Scale Factors . . . . .	12
3.2. Multiplier-Accumulator Board . . . . .	13
3.2.1. The Sequencer . . . . .	14
3.2.2. The Extended Accumulator . . . . .	15
3.2.3. End-of-Conversion Combiner Circuit . . . . .	15
3.2.4. Interface with Microcomputer . . . . .	16
3.2.5. Mode Control . . . . .	16
3.3. Noise Considerations . . . . .	17
3.3.1. Grounding . . . . .	17
3.3.2. Optical Isolation . . . . .	18
3.3.3. Power Supplies . . . . .	18
3.4. Other Hardware Changes . . . . .	19
3.4.1. 12-bit Input Modules . . . . .	19

3.4.2. DMA Board . . . . .	19
3.4.3. Frequency Counter and Programmable Time-Delay Board . . . . .	19
4. Software Changes . . . . .	20
4.1. Software Changes for IEEE 488 Interface . . . . .	20
4.2. Software Changes for HASW Upgrade . . . . .	23
5. Performance . . . . .	24
Acknowledgments . . . . .	27
References . . . . .	28
Appendix - Drawings . . . . .	A
Drawing 1 Basic Block Diagram of HASW . . . . .	A1
Drawing 2 Basic Block Diagram of Converter Modules . . . . .	A2
Drawing 3 Block Diagram of Amp/Data Converter Modules . . . . .	A3
Drawing 4 Block Diagram & Power Supply . . . . .	A4
Drawing 5 Clock-Synchronizer Board . . . . .	A5
Drawing 6 ADC Board 1 (Analogic) . . . . .	A6
Drawing 7 ADC Board 2 (Crystal) . . . . .	A7
Drawing 8 16-bit Amp/Data Curr. & Volt Conv Modules, Mother Board . . . . .	A8
Drawing 9 Current Transformer Schematic . . . . .	A9
Drawing 10 Current-to-Voltage Converter Board . . . . .	A10
Drawing 11 Multiplier-Accumulator - Block Diagram 1 . . . . .	A11
Drawing 12 Multiplier-Accumulator - Block Diagram 2 . . . . .	A12
Drawing 13 16-bit Mult-Acc Board - Part A and Part B . . . . .	A13
Drawing 14 16-bit Mult Acc Board - Board Layout Schematic . . . . .	A14
Drawing 15 Sequencer Timing Diagram . . . . .	A15
Drawing 16 End-of-Conversion Combiner Circuit . . . . .	A16
Drawing 17 Ground Connection Schematic . . . . .	A17
Drawing 18 System Power Supply Block Diagram . . . . .	A18
Drawing 19 Time Delay Extension . . . . .	A19
Drawing 20 Frequency Counter and Programmable Time Delay Board . . . . .	A20

## List of Figures

	page
Figure 1 Simplified Diagram of Current-to-Voltage Converter . . . . .	11
Figure 2 Typical Distribution of Voltage Codes for Shorted Input. . . . .	24
Figure 3 Frequency Response of Current-Input Module . . . . .	25
Figure 4 Frequency Response of Voltage-Input Module . . . . .	25
Figure 5 Frequency Response of Power Measurements . . . . .	26

## List of Tables

	page
Table 1 Voltage-Input Module Features . . . . .	5
Table 2 Current-Input Module Features . . . . .	7
Table 3 Dimensions of Transformer Components . . . . .	8
Table 4 Magnetic Impedances and Scaling Error . . . . .	10
Table 5 The Approximate Scale Factors . . . . .	13
Table 6 Addresses for Buffer Register, R7 and Mode-Latch Register, R6 . . . . .	16
Table 7 Mode Summary . . . . .	17
Table 8 IEEE 488 Commands . . . . .	21
Table 9 Selection Menu and Default Values . . . . .	22
Table 10 Temperature Sensitivities for the Input Modules in parts in $10^6/^{\circ}\text{C}$ . . . . .	27



# NIST High-Accuracy Sampling Wattmeter

*Abstract* - A high-accuracy sampling wattmeter was developed at the National Institute of Standards and Technology (NIST) to investigate the feasibility of using waveform sampling techniques for making very accurate power measurements at frequencies from 50 Hz to 1000 Hz. The goal of this effort was to develop an instrument having a full scale measurement uncertainty over these frequencies of less than  $\pm 50 \mu\text{W/W}$ . The prototype instrument that came out of the development was used to demonstrate the accuracy achievable with the digital sampling method. The new high-accuracy sampling wattmeter was built around a wideband instrument developed earlier at NIST. The new wattmeter uses 16-bit analog-to-digital (A/D) converters and includes a two-stage current transformer in one of the input modules. This wattmeter operates with asynchronous sampling as did the previous wattmeter. The high accuracy is achieved by approximately synchronizing the interval over which samples are taken with the period of the input signal. Special care was taken to design input stages with a flat frequency response and low temperature sensitivity. The wattmeter has been calibrated using the NIST Audio-Frequency Power Bridge. The two instruments agreed to better than  $\pm 50 \mu\text{W/W}$ , of full scale, over the 50 Hz to 1000 Hz frequency range at a wide range of power factors.

## 1. Introduction

The NIST High-Accuracy Sampling Wattmeter (HASW) was designed and fabricated at the National Institute of Standards and Technology (NIST) to meet the need for a high-accuracy ( $\pm 50 \mu\text{W/W}$ ) power measurement of low-distortion power signals in the power frequency range (fundamental frequency of 50 Hz to 1 kHz) and to examine to what level of uncertainty the sampling method for power measurement can be extended. The operation and the performance of the HASW is described in this report. It is a second generation instrument, which uses portions of an earlier 12-bit Wideband Sampling Wattmeter [1,2]. This report also describes the changes made to the Wideband Sampling Wattmeter. The power measurement technique used in the new instrument is basically the same as that used in the earlier wattmeter: dual-channel sampling using commercial track-and-hold (T/H), analog-to-digital (A/D) conversion, real-time multiplication, and microcomputer control. The reports on the earlier wattmeter [1,2] should be used to understand the operation of those portions of the new wattmeter that were not changed and are not described in this report.

The HASW uses two opto-isolated plug-in input modules (channels) to sample the input voltage and current signals at sampling rates up to 75 kHz, using 16-bit A/D converters. A high-speed digital multiplier-accumulator is used to calculate the power in real time from a large number of

input signal samples. The real-time multiplier-accumulator, together with the microcomputer, allows the wattmeter to calculate the power by averaging a large number of samples. The wattmeter has a relatively constant uncertainty for signal frequencies from 50 Hz to 1 kHz. The wattmeter response for higher frequencies is primarily limited by the response of the input modules. A feature unique to the earlier wideband sampling wattmeter, and used on this new wattmeter, is the use of programmable time-delay circuits to compensate for differential time delay between the two input channels.

Section 2 describes the basic operating principles of the HASW. A brief description is given of the various circuit operations. Section 3 provides a detailed description of the new hardware that was designed and fabricated to achieve the performance of the new wattmeter. It also describes the changes that were made to the hardware of the earlier wattmeter that was not completely replaced. Schematics and the operation of the circuits are given for the new hardware: the amplifier and current-converter module, amplifier and voltage-converter module, and the multiplier-accumulator board. Schematics and explanations are also given for the following changes in the old hardware: the direct-memory-access (DMA) board and the frequency counter and programmable time delay board. Section 4 describes the changes to the software that were necessary for control of the new wattmeter. Section 5 describes the performance of the new HASW based on the comparison of its power measurement readings with the NIST Audio Frequency Power Bridge [3].

## 2. System Operation

### 2.1. Power Sampling Basics

Periodic power signals with a voltage at time  $t$  of  $v(t)$ , a current of  $i(t)$ , and having a period of  $T$  seconds contain an average power,  $P$ , of

$$P = \frac{1}{T} \int_0^T v(t) i(t) dt . \quad (1)$$

Sampling wattmeters calculate the average power by performing the integration numerically, eq (2). The input voltage and current waveforms are sampled simultaneously, converted to digital values, and the product of their digital values, the instantaneous power, is calculated. The average power is computed by averaging many samples of instantaneous power. If the voltage at time  $t_k$  is denoted as  $v(t_k)$  and the current as  $i(t_k)$ , then the approximate average power,  $W$ , is given by

$$P \approx W = \frac{1}{n} \sum_{k=0}^{n-1} v(t_k) i(t_k) , \quad (2)$$



where  $n$  is the number of samples used in the average. The major error in determining the power,  $W$ , comes from the limitations inherent in the sampling process, and the imperfections of the hardware used to make the measurements [4 to 7]. Section 5 discusses the errors due to limitations of the hardware.

## 2.2. General Operation

This Section presents a brief description of the principle blocks of the HASW, and how they perform the power measurement operations. Drawing 1 is a simplified block diagram of the HASW. The voltage and current signals are sampled and converted to 16-bit digital quantities in the two input modules. The input signals are also scaled to produce the two opto-isolated analog outputs, trigger 1 and trigger 2 signals. The two 16-bit digital samples are sent to the multiplier-accumulator and to the DMA circuit, and the two trigger signals are sent to the interval control circuitry. The interval control circuit synchronizes the summation period with the input signals and generates the sample command pulses that control the sampling rate. Although the summation interval is synchronized with the input signals, the sample command pulses are not. The sampling pulses are derived from a fixed, crystal-controlled oscillator, and their repetition rate can be selected by the front panel keyboard. The microcomputer controls the summation interval, reads the data from the multiplier-accumulator, calculates the average power, displays the results and the wattmeter parameters, and interfaces with the operator through the keyboard. The summation interval is controlled to preserve high accuracy independent of the input signal frequency and of the sampling rate.

The programmable delay circuit enables setting a time difference between the voltage- and current-sample command pulses. The delay compensates for the differences in response of the two input channels and preserves the sampling accuracy. The DMA circuit saves 4096 samples of the two input signals. These samples are used for calculating the average and rms voltage and current.

## 3. Hardware Changes<sup>1</sup>

This section describes the operation and the performance of the new hardware and the changes that were made to the existing hardware. It also provides schematics and explanations for the various circuits. The new hardware (Drawing 1) consists of the amplifier and the 16-bit voltage-converter module, the amplifier and the 16-bit current-converter module, and the multiplier-accumulator board. The existing hardware to which changes were made are the DMA board and the frequency counter and programmable time delay board. The modifications to the earlier two

---

<sup>1</sup> This document reports on equipment developed at the National Institute of Standards and Technology. Certain commercial components are identified in order to adequately describe the design and operation of the equipment. Such identification does not imply recommendation or endorsement by the National Institute of Standards and Technology nor does it imply that the components are necessarily the best available for the purpose.

12-bit input modules to enable their use with the new HASW are also described. The last part of this Section discusses the efforts to reduce the induced noise and to improve the system performance, including the layout of the ground planes, the opto-isolation of the input module's front end, and the independent power supplies.

### 3.1. Amplifier and Conversion Modules

The current and voltage-input modules provide the interface and the impedance transformation for converting the analog voltage and current signals into 16-bit binary digital words. Drawing 2 shows the basic block diagram of the current-input module. Each of the modules includes a mother board, a plug-in A/D converter card and a plug-in clock-synchronizer card. Both modules have input voltage ranges of 255 V rms, 127 V rms, and 3 V rms ( $\pm 4.5$  V peak). The current-input module includes a two-stage current transformer and a current-to-voltage (I/V) converter card that give it additional current ranges of 5.5 A rms, 1.1 A rms, and 50 mA rms.

The voltage attenuators and the two-stage transformer and I/V converter card have an output signal in the range of  $\pm 4.5$  V peak. This signal is buffered with a unity-gain instrumentation amplifier. The output of the amplifier is connected to the A/D converter and to the opto-isolation amplifier. The isolated analog output is used to synchronize the sampling summation interval with the input signal (trigger 1 or trigger 2). Drawings 2, 3, and 4 show that the front end of the input module is opto-isolated from the main system. This feature reduces the noise introduced by any ground loop currents, enables the front end to float to the potential of the input power signals, and separates the noisy oscillator synchronizer circuit from the front end.

The plug-in A/D converter cards holds the A/D converter, the 4.5 V dc reference voltage, two DC/DC converters for  $\pm 5$  V dc, the data latch, and the circuitry for the delay and the strobe signals to the mother board. The plug-in clock-synchronizer card (Drawing 5) includes an oscillator and a synchronizing circuit. The clock-synchronizer provides the clock pulses to the A/D converter board. The synchronization circuit allows for the option of synchronizing the Hold command to the A/D converter with the rising edge of the clock signal, in response for each Sample (SMPL) command input initiated by the frequency counter and programmable time-delay board.

#### 3.1.1. Voltage Inputs

The voltage-mode specifications for the voltage- and the current-input modules are the same. Table 1 gives a summary of the features for the voltage inputs.

Referring to Drawings 6 and 7, the calibration ( $\pm 4.5$  V peak) input is protected by a 1/16 A fuse because it is connected directly to the input of the instrumentation amplifier. The two other voltage inputs are not protected, assuming that the RC voltage attenuators at the input to the instrumentation amplifier, the 200  $\Omega$  resistor in series with the output of the instrumentation

amplifier, and the two limiting diodes across the input to the A/D converter provide sufficient protection.

**Table 1** Voltage-Input Module Features

Input Range	Input Impedance
$\pm 4.5$ V peak	$5 \times 10^{12} \Omega \parallel 6$ pF
127 V rms	$100 \text{ k}\Omega \parallel 10$ pF
255 V rms	$100 \text{ k}\Omega \parallel 10$ pF

#### 3.1.1.1. The Attenuator

Each of the two voltage attenuators (Drawing 8), are resistor-capacitor (RC) dividers. The resistors of both voltage dividers were selected so that the input impedance of the attenuator is about  $100 \text{ k}\Omega$  at dc. The resistors have a specified temperature coefficient of  $10 (\mu\Omega/\Omega)/^\circ\text{C}$ , the capacitors have a specified temperature coefficient of  $30 (\mu\text{F}/\text{F})/^\circ\text{C}$ , and the adjustable capacitors are piston-air capacitors. The adjustable capacitors are used to give a flat response over the frequency range of interest. The capacitors are adjusted so that the wattmeter gives the same reading for a 4 kHz input voltage as for a 50 Hz input voltage.

#### 3.1.1.2. Instrumentation Amplifier

The instrumentation amplifier (Drawing 8), U19, serves as a unity-gain buffer to drive the analog input of the A/D converter and the analog opto-isolated amplifier, U1. U19 was selected because of its good temperature stability, low noise, low offsets, high common-mode rejection ratio (CMRR) and high input impedance (noise =  $0.3 \mu\text{V}_{\text{pp}}$ ,  $V_{\text{os}} = 0.05 \text{ mV}$ ,  $I_{\text{os}} = 10 \text{ nA}$ ,  $\Delta V_{\text{os}} = 0.5 \mu\text{V}/^\circ\text{C}$ , CMRR = 120 dB, bandwidth = 1 MHz, differential input impedance =  $5 \times 10^{12} \Omega \parallel 6$  pF, and common-mode input impedance =  $2 \times 10^{12} \Omega \parallel 1$  pF). Even though the bandwidth of U19 is only 1 MHz, it is adequate for analog input signals in the 50 Hz to 1 kHz range.

For testing purposes, jumpers can be used to change the normal signal flow in the input modules. With various jumpers, the front-end signal can bypass the instrumentation amplifier, the input ground of the instrumentation amplifier can be connected or separated from its output ground, and the input to the A/D converter can be shorted to its input ground. For normal operation the front-end signal passes through the instrumentation amplifier, and the input and output ground of the amplifier are connected to the A/D analog ground. To enable offsetting the instrumentation amplifier, U19, from the front panel, a plastic rod connects the offset potentiometer's P1 setting screw to the front panel.



### 3.1.1.3. A/D Converter Cards

Two pairs of plug-in A/D converter cards (Drawings 6, 7) were fabricated. One pair uses ADC4203 A/D converters from Analogic, and the other pair uses CS5101 A/D converters from Crystal. The ADC4203's maximum sampling rate is 40 k samples per second while the CS5101 can be operated at up to 80 k samples per second. To enable the A/D converters to operate at their maximum sampling rates, the ADC4203 needs a 4 MHz clock and the CS5101 needs an 8 MHz clock. The plug-in clock-synchronizer card provides the clock pulses. For each A/D converter type, the appropriate crystal oscillator is plugged into the clock-synchronizer card. Each pair of converters uses the same input signals from the mother board and generate similar output signals (16-bit two's complement data and strobe signals). The analog input voltage to the A/D converters is protected by two clamping diodes D1 and D2.

The converter cards include: a  $\pm 5$  V power supply, a 4.5 V reference source for the A/D converters, and the circuitry needed for data latching and generating the strobe signals.

#### A. Timing Signals

The two timing signals to the A/D converter board, CLK and HOLD, are generated by the clock-synchronizer card (Drawing 5). By placing the clock-synchronizer card away from the A/D converter card and eliminating a common ground between these cards by opto-isolation, the clock noise induced on the input signal is reduced considerably. The falling edge of the Hold signal places the internal track-and-hold circuit of the A/D converter in the hold mode and initiates an analog-to-digital conversion cycle. The CLK signal is a TTL-level square wave signal. The signal is fed into the clock input of the A/D converter to synchronize its conversion cycle. The frequency of the CLK signal is determined by the crystal oscillator chip used (Drawing 5, U1). For the ADC4203 A/D converter, a 4 MHz oscillator is used. For the CS5101 A/D converter, an 8 MHz oscillator is used.

#### B. Output Data and Signals

The two output control signals from the A/D converter card, EOC-OUT and CLK1, (Drawings 6 and 7) indicate the end of a conversion cycle. On the rising edge of CLK1 the 16-bit data from the A/D board is latched into registers U7 and U8 on the mother-board. The rising edge of EOC-OUT signals the system that the data are ready to be read. The EOC-OUT signal and the data are passed to the system's multiplier-accumulator board via opto-isolators (U5, U9 to U17).

#### C. The 4.5 V DC Reference Source

The voltage reference circuit recommended by Crystal was implemented on the A/D converter boards. The value of the dc reference source (4.5 V) determines the maximum analog input signal level ( $\pm 4.5$  V peak) and the scale of conversion. The dc reference-source output impedance and

regulation frequency response matches the power input impedance of the A/D converter. This impedance matching reduces the noise induced in the conversion from changes in power consumed by the A/D converter during the conversion cycle.

#### D. The CS5101 A/D Converter Card

The CS5101 converter (Drawing 7) clocks the 16-bit two's complement data serially (the most significant bit first and the least significant last) through the output SDATA during conversion. The output SCLK provides 16 synchronized pulses for latching the data. Two shift registers, U5 and U6 in cascade, provide a 16-bit shift register to collect and store the data for each conversion. The output SDATA is connected to the input of the shift register and output (SCLK) is connected to the clock input of the two shift register devices. After the data are stored in the 16-bit shift register, the output TRK1 goes from high to low, signaling the end of conversion and that the data are ready to be read. The output TRK1 is inverted and fed to the one-shot U4A. At the end of conversion, U4A provides the CLK1 and the EOC-OUT signals to latch the data into the registers on the mother board and to signal the multiplier-accumulator board that the data are ready to be read.

#### E. The ADC4203 A/D Converter Card

The ADC4203 A/D converter (Drawing 6) latches the 16-bit two's complement data into an internal tri-state buffered register. The outputs of the shift register, U6, provide the pulses for retrieving the data. The output EOC\ is connected to the input of U6 and the master clock signal, CLK, is connected to the clock input of U6. At the end of conversion, the output EOC\ goes from high to low for a period of about 24 master clock cycles. The output C0 of U6 is connected to the input RD\ to enable the internal register of the A/D converter. The outputs C3 and C6 provide for CLK1 and EOC-OUT output signals.

### 3.1.2. Current Inputs

Table 2 gives a summary of the features of the current-mode inputs available on the current-input module. All three current-input ranges are fuse protected. The input impedance of each of the three ranges is the resistance of the corresponding protection fuse measured at room temperature.

Table 2 Current-Input Module Features

Input Range	Input Impedance
50 mA	6.12 $\Omega$ (0.1 A fuse)
1.1 A	85 m $\Omega$ (1.5 A fuse)
5.5 A	34 m $\Omega$ (6 A fuse)

### 3.1.2.1. Two-Stage Input Transformer

The two-stage input transformer is used to scale down the input current to  $\pm 50$  mA full scale. The output current of the transformer is fed into the I/V converter card. The use of a two-stage transformer [8] reduces the error introduced by scaling down the input current. The benefits of using an input transformer are the isolation that it provides and the ease of use by eliminating the need for a low-value, high-power shunt resistor. The disadvantage is that the module can not measure dc current. Drawing 9 shows the schematic representation, the equivalent circuit, the construction of the two-stage transformer, and some set-ups for measuring the two-stage transformer parameters.

Two identical torus-shaped cores with a square cross section (core one and core two) having the Magnetics model number AK026 50103-4F, and a torus-shaped magnetic shield box with a square cross section, made of a high-permeability material, were used for fabricating the two-stage transformer. Table 3 gives the dimensions of the components used to make the transformer.

Table 3 Dimensions of Transformer Components

	ID	OD	Height
Core	2.00" (50.8 mm)	3.00" (76.2 mm)	0.50" (1.27 mm)
Case	1.94" (49.3 mm)	3.13" (79.5 mm)	0.63" (1.60 mm)
Shield	1.38" (35.1 mm)	3.50" (88.9 mm)	0.75" (1.91 mm)

The tertiary winding (100 turns of a 16-gauge wire) and the cascade winding (one turn of a 20-gauge wire) were wound on core two, then core two was placed into a two-part magnetic shield. To eliminate the shield from forming a closed one-loop winding, the inner diameter of the two halves of the shield are isolated as indicated in Drawing 9 by a bigger gap. Core one was placed on top of the magnetic shield and the secondary winding (100 turns of 18-gauge wire) was wound around core one, core two, and the magnetic shield. The two primary windings were wound over the secondary winding. One primary winding is for the 5.5 A range (one turn formed from five turns wired in parallel), and the other is for the 1.1 A range (five turns of 14-gauge wire). The scale-down ratios of the 1.1A and the 5.5A input ranges are 20:1 and 100:1, respectively.

To confirm that the tertiary and the secondary windings both have the same number of turns, the two windings were connected in series to a source in a manner that their flux contributions cancel (Drawing 9). Because of the construction of the transformer (the windings of the secondary include the winding of the tertiary), the flux through the tertiary is very small when both windings

have the same number of turns. Therefore, a voltmeter connected across the tertiary should measure a small reading. By adding or subtracting one turn from the secondary, it can be verified whether the number of turns is equal.

To cascade the input transformer to an external two-stage transformer for increasing the range of the current to be measured, the secondary and the tertiary windings of the external transformer can be connected to the one-turn primary and to the one-turn cascade winding of the input transformer. Because the cascade winding is a one-turn winding, it can be combined only with the one-turn primary winding (range 5.5 A) of the input transformer. The magnetic shield is connected to the front panel through the connector labeled Trans. Guard. Grounding this connector reduces the capacitive coupling of common-mode signals to the wattmeter.

The two-stage transformer is connected such that the current to be scaled,  $I_p$ , is applied to the primary of the transformer and the scaled output current is the sum of the currents in the secondary,  $I_s$ , and the tertiary,  $I_t$ , windings. The scaling ratio ideally should be the ratio of the number of turns of the primary,  $N_p$ , to the number of turns of the secondary winding,  $N_s$ , which is equal to the number of turns of the tertiary winding,  $N_t$ . The scaling error of the two-stage transformer,  $\epsilon$ , is the deviation of the ratio from this ideal. This error is given as

$$I_s + I_t = I_p \frac{N_p}{N_s} (1 - \epsilon) . \quad (3)$$

The scaling error can be calculated by using the equivalent circuit [8] to calculate the sum of the secondary and tertiary currents. The sum is given as

$$I_s + I_t = I_p \frac{N_p}{N_s} (1 - \epsilon_s \epsilon_t) , \quad (4)$$

where  $\epsilon_s$  and  $\epsilon_t$  are the error if the secondary or the tertiary windings were used separately and are given by

$$\epsilon_s = \frac{Z_s + Z_{b1}}{Z_{m1}} , \quad (5)$$

and

$$\epsilon_t = \frac{Z_t + Z_{b2}}{Z_{m2}} . \quad (6)$$

$Z_s$  and  $Z_t$  are the impedances of the secondary and tertiary windings,  $Z_{m1}$  and  $Z_{m2}$  are the magnetic impedances of core one and two, and  $Z_{b1}$  and  $Z_{b2}$  are the burden impedances for the secondary and tertiary windings. The magnetic impedances are described below.

It should be mentioned that the errors introduced by the various capacitances (between the



windings and the windings to the ground) and the eddy current were not considered. To take those errors into consideration a more elaborate equivalent circuit is needed.

From eqs (5) and (6) it is clear that the scaling error can be reduced by shorting the outputs of the secondary and the tertiary, reducing the winding resistances (the real part of  $Z_s$  and  $Z_t$ ), and choosing cores that yield a high magnetic impedances ( $Z_{m1}$ ,  $Z_{m2}$ ) [8].

The magnetic impedance is a function of the core dimensions, the frequency, and the relative initial permeability and is given by

$$\frac{Z_m}{N^2} = \frac{4 \pi 10^{-7} \mu A \omega}{l}, \quad (7)$$

where  $Z_m$  is the magnetic impedance,  $N$  is the number of turns,  $\mu$  is the initial permeability,  $A$  is the cross section of the core,  $\omega$  is the input signal frequency, and  $l$  is the mean path length of the magnetic flux inside the core. Assuming the relative initial permeability,  $\mu$ , is  $6 \times 10^4$ , the input signal frequency,  $\omega$ , is 60 Hz, and the number of turns,  $N$ , is 100, then by eq (7) the calculated magnetic impedances of the two-stage input transformer,  $Z_{m1}$  and  $Z_{m2}$ , are about 200  $\Omega$ . After fabrication, the resistances of the windings and the magnetic impedances of the transformer were measured for frequencies of 50 Hz, 1 kHz and 10 kHz and the measured values are about two times the calculated values. The dc resistance of the secondary is about 0.3  $\Omega$  and that of the tertiary is about 0.1  $\Omega$ . The measured impedance values and scaling errors are shown in Drawing 9 and summarized in Table 4.

As can be seen from Table 4, the scaling errors caused by the winding resistance are negligible. For 1 kHz and higher frequencies, the errors caused by the stray capacitances and the eddy current are probably dominant and much more than those caused by the winding's impedance.

Table 4 Magnetic Impedances and Scaling Error

Freq. (Hz)	$Z_{m1}$ (Ohms)	$Z_{m2}$ (Ohms)	Scaling Error (parts in $10^6$ )
50	450	433	0.2
1 k	2.5 k	2.5 k	negligible
10 k	12 k	12.5 k	negligible

### 3.1.2.2. I/V Card

A schematic of the current-to-voltage (I/V) converter circuit is shown in Drawing 10. The basic I/V circuit, shown in Figure 1, consists of the feedback resistor and capacitor,  $R_f$  and  $C_f$ ,



a compound amplifier (identical amplifiers A1 and A2), the resistive attenuator  $R_1$  and  $R_2$ , and the RC attenuator  $R_a$  and  $C_a$ . The resistive attenuator is necessary to prevent oscillations and its attenuation should be set to the lowest possible ratio that gives a minimum reduction in the compound amplifier's gain, as explained below.

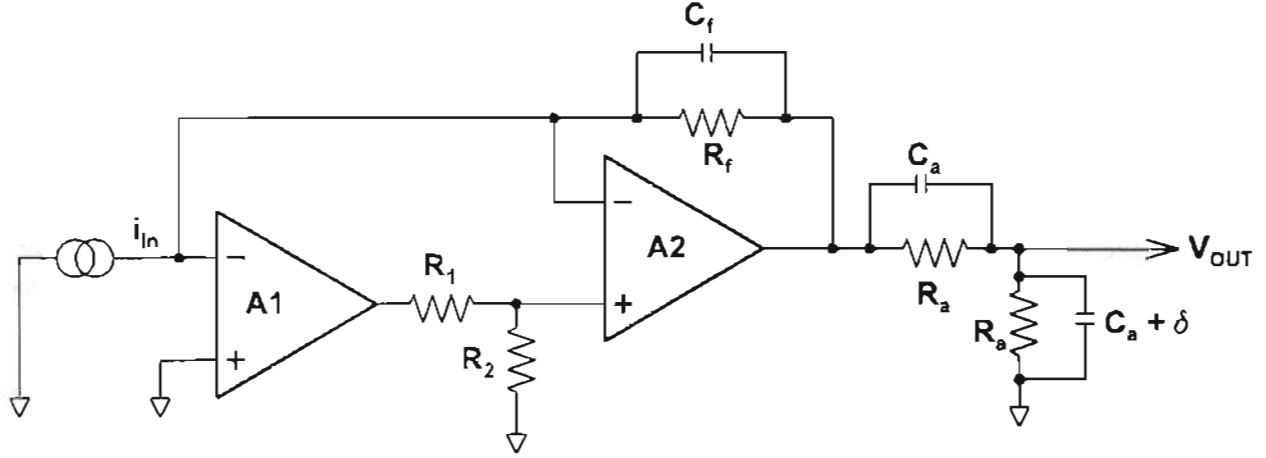


Figure 1 Simplified Diagram of Current-to-Voltage Converter.

The transfer function  $G$  of the I/V converter relates the output voltage,  $V_{out}$ , to the input current,  $I_{in}$ , as  $V_{out} = G I_{in}$ . An approximation of  $G$  is given by

$$G \approx - \frac{1}{1 + j \omega R_f C_f} R_f \frac{1 + j \frac{\omega}{\omega_t \rho}}{1 - \frac{1}{\rho} \left( \frac{\omega}{\omega_t} \right)^2 + j \frac{\omega}{\omega_t \rho}} \frac{(1 - j 0.5 \omega R_a \delta)}{2}, \quad (8)$$

where  $\omega$  is the input signal frequency,  $\omega_t$  is the unity gain frequency of A1 and A2,  $\delta$  is the incremental capacitance added to the lower portion of the RC attenuator,  $R_a$  and  $C_a$  are the values of the upper and the lower portions of the RC attenuator, and  $\rho$  is given by

$$\rho = \frac{R_2}{R_1 + R_2}. \quad (9)$$

The approximation for  $G$  is valid provided that  $\omega$ ,  $\delta$ , and  $\rho$  are such that

$$(\omega R_a C_a)^2 \ll 1, \quad \delta \ll C_a, \quad \text{and} \quad \frac{1}{\rho} \left( \frac{\omega}{\omega_t} \right)^2 \ll 1. \quad (10)$$

The first factor of the expression for  $G$  represents the effects of the feedback capacitor,  $C_f$ . The second factor describes the effects of the finite bandwidth,  $\omega_t$ , of the amplifiers A1 and A2 and

the resistive attenuator,  $R_1$  and  $R_2$ . In the frequency range that satisfies the third inequality in eq (10), the denominator and numerator of this factor cancel each other and the response from this factor is very close to the dc gain, which is  $R_f$ . The third inequality of eq (10) also indicates that the frequency range for a flat response increases as the value of the divider ratio,  $\rho$ , goes higher. For the HASW design,  $\rho$  was set to the value of 0.001. The third factor of the expression for  $G$  represents the effect of unbalancing the RC voltage divider by adding a small capacitance,  $\delta$ , in parallel to its lower portion (small meaning that the second inequality of eq (10) is satisfied). The first and third factors show that  $C_f$  and  $\delta$  produce very similar effects on the transfer function; thus, either approach can be used to adjust the time delay of the circuit. Since the RC voltage attenuator is a part of both the current and voltage sections of the current-input module, the method used for the HASW was to use the feedback capacitor,  $C_f$ , to adjust the time delay of the current inputs and the RC voltage attenuator to adjust the time delay of the voltage inputs. It was found experimentally that the overall response of the HASW is best if  $C_f$  is set to 15.9 nF.

### 3.1.3. Clock-Synchronizer Card

The clock-synchronizer card (Drawing 5) supplies the A/D converter with the master clock pulses. By plugging the proper oscillator into the card, it supplies a 4 MHz clock to the A/D board with the ADC4203 converter or 8 MHz to the A/D converter with the CS5101 converter. The other function of the board is to synchronize the input sample (SMPL) command from the frequency counter and the programmable time-delay board with the master clock. When jumper JM3-4 is set for the synchronizing (SYNC) mode, for each SMPL command a synchronized positive HOLD pulse is emitted, signaling the A/D converter to start a conversion. The resolutions of the A/D converters are verified for the SYNC and the unsynchronized (DIR) modes. Both A/Ds converters produce a smaller spread in the codes under the DIR mode. For that reason the board is set to the DIR mode.

The clock-synchronizer board is plugged into the lower side of the mother board. It is thus shielded from the A/D converter by the systems ground plane, as part of the efforts to minimize the induced noise to the analog-to-digital conversion portion of the input modules. To eliminate more noise induced by the oscillator, this board's ground is separated from the A/D converter board's ground, and the master clock and the HOLD command are transferred to the mother board via opto-couplers.

### 3.1.4. Scale Factors

The analog input voltages or currents are transformed into a voltage,  $V_{in}$ , which is applied to the A/D converter for conversion to a corresponding digital word. Each voltage input has a particular gain,  $G_v$ , and each input current has its particular transconductance,  $G_i$ . The 16-bit number  $N$  is the digital value of  $V_{in}$  scaled to the reference voltage,  $V_{ref}$ , by the A/D converter. For numerical calculation,  $N$  has to be multiplied by a scale factor,  $S$ , to determine the value of the

analog input signal. The input current,  $I_{in}$ , is given by  $I_{in} = S_i N$  and the input voltage,  $V_{in}$ , is given by  $V_{in} = S_v N$ . For the HASW the approximate scale factors in terms of the least significant bit (lsb) of the converter are given by

$$S_v = \frac{V_{ref}}{2^{n-1}} \frac{1}{G_v} \approx \frac{4.5}{2^{15}} \frac{1}{G_v}, \quad (11)$$

and

$$S_i = \frac{V_{ref}}{2^{n-1}} \frac{1}{G_i} \approx \frac{4.5}{2^{15}} \frac{1}{G_i}. \quad (12)$$

The approximate scale factors for the various ranges are given in Table 5.

**Table 5** The Approximate Scale Factors

Input Range	Approximate Scale Factor
Voltage Cal., 4.5 V	137.5 $\mu$ V/lsb
127 V	5.488 mV/lsb
255 V	10.985 mV/lsb
Current Cal., 50 mA	2.29 $\mu$ A/lsb
1.1 A	45.8 $\mu$ A/lsb
5.5 A	229 $\mu$ A/lsb

### 3.2. Multiplier-Accumulator Board

The multiplier-accumulator board multiplies the digitized current and voltage values and sums the resultant products. At the end of the hardware accumulation period, the sum is stored in a latch and an interrupt is sent to the microcomputer. Drawing 11 shows a general block diagram of the multiplier-accumulator board and Drawing 12 shows a second block diagram with more details of the sequencer, which controls the operation of the multiplier-accumulator, and additional details of the extended accumulator. The circuits are shown in Drawings 13, and 14. The hardware accumulation period is controlled by the terminal count, TC, signal produced by the frequency counter and programmable time-delay board. The multiplying and summing of the sampled data is controlled by the pulses generated by the sequencer. The arithmetic operations are carried out in a high-speed multiplier-accumulator (LSI device TDC1010J). This device contains a 16-bit by 16-bit multiplier, a 35-bit accumulator, and an internal latch.

The multiplier-accumulator board has four modes of operation. The mode controls which data are multiplied and summed on the board. Depending on the mode, the board accumulates either power products, voltage values, current values, or sample counts. The operation of the sequencer, the extended accumulator, and other support circuitry on the multiplier-accumulator board are described in the following sections.

### 3.2.1. The Sequencer

The sequencer controls the operation of the multiplier-accumulator board by generating a series or cycle of pulses after receiving a start sequence pulse, SEQ, from the end-of-conversion combiner circuit. The sequencer produces three different pulse cycles, depending on the terminal count (TC) pulse from the frequency counter and programmable time-delay board. The initial cycle starts the hardware accumulation period by clearing the accumulator, R3 (Drawing 12), and latching into it the first product of the sampled data of the new accumulation period. The normal cycles that follow each of the next data conversions add the product of the sampled data to the accumulator, R3. Upon receipt of the TC pulse, the sequencer generates the terminal cycle that adds the last product of the hardware accumulation period into the accumulator, R3, latches the accumulator data into the buffer register, R7, and sends an interrupt to the microcomputer. The sequencer starts the next hardware accumulation period at the next data conversion by generating the initial cycle pulses.

The timing diagram (Drawing 15) of the sequencer shows three cycles, the first one is the last normal cycle (designated by N-1) of a hardware accumulation period, the second (designated by N) is a terminal cycle and the third one is the initial cycle (designated by 1) of the next accumulation period. As can be seen, for every cycle the train of pulses, C0 to C11, are initiated by the SEQ signal. The TC signal, together with the CEOC signal, control the initiation of a terminal cycle followed by an initial cycle of the next hardware accumulation period. The differences between the three different cycles is related to the control signals LTC, ACC, TSL, and the conditional signals, CCn, that are also produced by the sequencer. The LTC signal is derived from TC and CEOC signals and it controls the terminal cycle by enabling the various conditional pulses CCn that latch the data accumulated during the hardware accumulation period into the buffer register, R7, which is accessible by the microcomputer. The ACC signal is initiated by the falling edge of the LTC signal, and by going low, it enables the initial cycle to clear the accumulator, R3. The TSL signal controls data multiplexing of the common outputs of the least significant product (LSP) buffer and register R5. This multiplexing enables either the output data of register R5 to be latched into register R2 or enables the data in the accumulator, R3, to be latched into the buffer register, R7.

Two shift registers connected in series, R8, that are clocked by an 8 MHz oscillator, are used to generate the positive pulse train, C0-C11. Each of the Cn pulses has a duration of 250 ns and the time difference between the rising edge of each successive pulses is 125 ns. The CCn (conditional) pulses, which are derived from the Cn series, are generated only during the terminal cycle for

latching the content of the accumulator, R3, into the buffer register, R7, (multiplier-accumulator output data latch).

### 3.2.2. The Extended Accumulator

The internal accumulator, R3 (Drawing 12), of the multiplier-accumulator device TDC1010J is 35 bits wide. It can only accumulate the sum of sixteen 16-bit by 16-bit products when each multiplicand has the maximum value in two's complement notation before overflowing. To overcome this limitation an accumulator extension was added. To implement the extension, it is necessary to detect the overflows and the underflows of the accumulator, R3, and to increment or decrement accordingly an external binary counter. An overflow is characterized by the transition from high to low of the two most significant bits (P33, P34) of R3 and an underflow is characterized by the transition from low to high of the same bits. The two D flip flops, U21A and U21B, hold the previous values of bits P33 and P34. By connecting the outputs of U21A and U21B, and the inverse of bits P33 and P34 into the input of the NAND gate, U23A, its output will switch from high to low when an overflow of R3 occurs. Similarly, by connecting the inverted outputs of the D flip flops, U21A and U21B, and the bits, P33 and P34, to the input of U23B, its output will switch from high to low when an underflow of R3 occurs. U24, U25, and U26 are three 4-bit up/down binary counters cascaded together to form a 12-bit binary counter. The counter is enabled whenever an underflow or overflow occurs by connecting the output of the NAND gate U31B to the ENT and ENP inputs of the first counter, U24. The U/D input of all the counters is connected to the output of the NAND gate, U23B, thus counting up when an overflow occurs and counting down when an underflow occurs. The count-up or down occurs on the rising edge of the C7 pulse of the sequencer. At the beginning of each hardware accumulation period, the sign of R3 has to be transferred to the extension. To accomplish this, all the data inputs of the three counters are connected together through NAND gate buffer, U31C, to the MS bit, P34 of R3. During the first cycle of every hardware accumulation period the ACC signal is low, thus enabling storing the product in R3, and also loading the value of bit P34 into the extension counters on the rising edge of the C7 pulse. To get the right values, the extension should never overflow or underflow. Adding 12 bits to the accumulator, R3, brings the total capacity to 47 bits and that enables it to sum at least 65,536 16-bit by 16-bit products without overflow or underflow.

### 3.2.3. End-of-Conversion Combiner Circuit

The end-of-conversion (EOC) combiner circuit (Drawing 16) enables the use of two different input modules with different A/D conversion times. When a sequence of a sample SMPL command followed by an end-of-conversion (EOC) signal from each input module are detected by this circuit, it sends the output signals, SEQ and CEOC, to the sequencer circuit, and the DMA-EOC signal to the DMA board, to indicate that a pair of 16-bit sampled data are ready.



### 3.2.4. Interface with Microcomputer

At the end of each hardware accumulation period the buffer register, R7, of the multiplier-accumulator board (Drawing 12) interrupts the microcomputer to retrieve its contents, which is a 47-bit two's complement number. These data are stored in six 8-bit registers (five AM25LS2520 and one 8212). Since the data bus is 8 bits wide, the microcomputer must address R7 six times, and reconstruct the data based on the retrieved byte's addresses. To change the mode of operation of the multiplier-accumulator board, the microcomputer writes the new mode byte into the mode-latch register, R6. Table 6 summarizes the addresses of registers R6 and R7. The addresses of the registers comprising R7 are listed from the least significant byte (LSB) to the most significant byte (MSB).

Table 6 Addresses for Buffer Register, R7 and Mode-Latch Register, R6

Register R7 Read Address	Component Drawing 13
0E0 Hex LSB	U20
0E2 Hex	U19
0E4 Hex	U18
0E6 Hex	U17
0E8 Hex	U28
0EA Hex MSB	U27
Register R6 Write Address	Component Drawing 13
0E4 Hex	U5

### 3.2.5. Mode Control

The multiplier-accumulator board (Drawings 12, 13) can operate in four modes designated 0, 1, 2, and 3. The mode controls which data are latched into registers R4 and R5 on the rising edge of the C0 pulse at the beginning of each multiply accumulation cycle. Table 7 summarizes the values of the data that are latched into R4 and R5 for each mode. For power measurement the system uses mode 0, which is the default mode when the system is powered up. The mode can be changed by the front panel keyboard. When the system detects a mode-change request, an 8-bit word is written into register R6.

**Table 7 Mode Summary**

Mode	R4 latched data	R5 latched data
0	16-bit channel 1 data	16-bit channel 2 data
1	Numerical value 1	16-bit channel 2 data
2	16-bit channel 1 data	Numerical value 1
3	Numerical value 1	Numerical value 1

The quantity measured depends on the mode of the multiplier-accumulator board. For mode 0 the output reading is power; for mode 1 the output is the average of the channel two signal level; for mode 2 the output is the average of the channel one signal level. For mode 3 the output is the numerical value 1, which indicates that the frequency counter and programmable time delay board is measuring the same number of samples during each multiply and accumulation period as the multiplier-accumulator board. Modes 1 and 2 are used to measure the offsets of the input modules.

### 3.3. Noise Considerations

In this section, some design features of the system that are associated with the effort to reduce noise will be addressed: the ground planes, opto-isolation, and power supplies.

#### 3.3.1. Grounding

There are six principle ground planes in the HASW system (Drawings 4, 17, and 18). Five of them follow the main blocks of the system: the microcomputer, the voltage-module digital circuitry, the voltage-module analog circuitry, current-input-module digital circuitry, and the current-input module analog circuitry. The sixth ground is the chassis ground. Some grounds are connected together at selected locations to reduce noise.

The six ground planes are referenced by the following names:

- a. The chassis ground (CHS GND).
- b. The system ground plane (SYS GND).
- c. The voltage-input module digital ground plane (DGTL GND).
- d. The voltage-input module analog ground plane (ANLG GND).
- e. The current-input module digital ground plane (DGTL GND).
- f. The current-input module analog ground plane (ANLG GND).

The CHS GND consist of the cabinet and the case of all the assemblies that are located within it.

This ground is connected to the ground pin of the power plug. The SYS GND is the ground plane of the microcomputer mother board and the plug-in boards (Drawing 18). The SYS GND and the CHS GND are connected together at the point where the microcomputer power supply crate is attached to the cabinet. Each of the input modules include three ground planes, the ANLG GND, and the DGTL GND of that module, and the SYS GND. All the input module components that are powered from the main system share the SYS GND. The DGTL GND and the ANLG GND of each input module are isolated from the CHS GND and from the SYS GND. The DGTL GND and ANLG GND of each module are isolated from the DGTL GND and ANLG GND of the other module. This isolation is achieved by using separate linear power supplies for each module (Drawing 4). The DGTL GND and the ANLG GND of each input module are connected together at one point on the back of the plug-in A/D converter card through jumper JP3 (Drawings 6 and 7). Using one point of connection is done to minimize the induced noise from the digital circuitry into the analog circuitry and particularly into the analog section of the A/D converter.

### 3.3.2. Optical Isolation

The two dotted lines through the opto-isolators, shown on the input module block-diagram (Drawing 3), indicates the boundary between the isolated analog front-end of the input module and the digital circuitry that interfaces directly with the microcomputer system. The opto-isolators, while transferring the digital and the analog signals, serve as high-impedance isolators that reduce the ground-loop currents. Another benefit of the opto-isolation is the convenience in use of the HASW due to the ability of the front-end input modules to float at the potential of the monitored system. The maximum allowable voltage difference between the front end and the system ground is 500 V.

### 3.3.3. Power Supplies

Every power supply common is connected to, and thus associated with, a ground plane (Drawings 4, 18).

The  $\pm 15$  V SYS AC/DC converter common is connected to the SYS GND and supplies power to the system side of the opto-isolated analog amplifier U1.

The +5 V SYS AC/DC converter common is connected to the SYS GND and it supplies power to

1. the EOC one-shot and associated components,
2. the clock-synchronizer card, and
3. the system side of the opto-isolators.

For each input module, the common of a  $\pm 15$  V ANLG AC/DC converter is connected to the ANLG GND of the input module and it supplies power to

1. the instrumentation amplifier, U3,



2. the current-to-voltage converter card (only on the current-input module),
3. the isolated input of the opto-isolated analog amplifier, U1, and
4. the A/D converter card.

For each input module, the common of a  $\pm 5$  V DGTL AC/DC converter is connected to the DGTL GND of the input module and it supplies power to

1. the data latch, R2,
2. the isolated-input front-end side of the opto-isolators, and
3. the digital circuits on the A/D converter card (the data latch R1, and the time delay and associated components).

The use of separate power supplies for the analog and the digital circuits of each of the input modules serves to reduce the noise induced onto the analog input signal and into the analog section of the A/D converter.

### 3.4. Other Hardware Changes

#### 3.4.1. 12-bit Input Modules

Two changes were needed to allow the previous 12-bit input modules to operate in the 16-bit environment. The first was to change the A/D converter output data into a 16-bit integer. The second was to change the 12-bit two's complement integer into a 16-bit integer by connecting the most significant bit (of the 12-bit integer) to the five edge-connector pins corresponding to the five upper bits of the 16-bit integer.

#### 3.4.2. DMA Board

The DMA board was originally built to accommodate 16-bit integers, except that its four most significant bits were connected together to accommodate the older 12-bit modules. The only change necessary was connecting each of those four bits separately to the 60-pin edge connector.

#### 3.4.3. Frequency Counter and Programmable Time-Delay Board

The frequency counter and programmable time-delay board (Drawings 19, 20) provides the Sample SMPL command pulses to the two input modules. To allow for differential time delays between these modules, the two pulses can be shifted relative to each other. Previously, the board could shift the channel-one sample command -60 ns to 200 ns relative to the channel-two sample command. This range was sufficient for the 12-bit input modules but not for the new 16-bit modules. The new modules require a relative time shift of about 800 ns. To achieve this longer delay, an additional programmable delay was introduced ahead of the two output programmable-delay components, PTTL-DL60-1 and PTTL-DL15-16, which were already implemented on the board. The output of the D flip flop, U9A, is connected to the input of the shift register, U39.

A 6 MHz clock is connected to the clock input of U39. The delay between consecutive outputs of the shift register is thus 166.6 ns. The outputs of the shift register are connected to the inputs of the multiplexer, U40. By setting switch SW2, a delay between 166.6 ns to 1333.3 ns can be selected. The table in Drawing 19 summarizes the switch, SW2, setups for the different delays and how to select the two channels.

## 4. Software Changes

The software in the HASW is a minor revision of the previous software used in the Wideband Sampling Wattmeter. This earlier software is extensively described in an NBS Technical Note [2]. The software description here will highlight the changes made in the two upgrades that have occurred to the software since that description. The first upgrade was to accommodate the addition of an IEEE 488 interface to the earlier wattmeter and the change in microcomputer used to control the wattmeter. The second software upgrade was the one made to accommodate the changes made for the HASW upgrade. The software is written in a combination of Pascal and assembly language. The assembly language software provides the interface to the hardware for the Pascal routines. Assembly routines are used to set and read the hardware registers and to respond to the interrupts. The Pascal routines provide the main control software of the wattmeter.

### 4.1. Software Changes for IEEE 488 Interface

The IEEE 488 interface is provided by the ZT 85/38 Multibus to IEEE 488 interface card from Ziatek Corp. The IEEE 488 address of this board is set via a dip switch on this board. Assembly language routines initialize and interface with this board, and Pascal routines read commands sent to the wattmeter and respond with wattmeter data and status.

As part of this general software upgrade, additional measurement capabilities were added to the earlier wattmeter, including direct access to the DMA contents as well as four additional measurement functions. Two arrays of the measurement values saved in the DMA can be sent on the IEEE 488 interface to an attached computer for further analysis. The number of values sent can be selected to be from 1 to 4096. The new measurement functions are energy, energy count, and clip count for channel 1 and channel 2. A new parameter was added in connection with the energy function, the clock correction factor. This factor corrects for the error in the frequency of the crystal that controls the sampling rate. The energy is displayed in Joules and the energy count gives the number of samples used in the currently displayed energy measurement. The two clip counts give the number of DMA stored values, which are at either the positive or negative saturation level. If these counts are not zero, then the measurement results are in error due to amplitude clipping of the input signals by the analog-to-digital converters.

The way many operational parameters are set via the software has been modified to make the control of the wattmeter easier. These modifications include the way the scale factors and delay times are

set for the two channels and the way functions are displayed on the wattmeter display. Also, new parameters have been added to control the way measurement data are sent over the IEEE 488 interface.

**Table 8 IEEE 488 Commands**

Char	Function	Char	Function	Char	Function
A	Up (↑)	a	na	1	1
B	Down (↓)	b	(Ar2End)	2	2
C	Left (←)	c	(MCh1SF)	3	3
D	Right (→)	d	na	4	4
E	Home	e	(Ar2End)	5	5
F	Run	f	(SampFreq)	6	6
G	FUp (F↑)	g	na	7	7
H	FDown (F↓)	h	na	8	8
I	na	i	(IntgPer)	9	9
J	na	j	(Ar1Beg)	0	0
K	DumpAr1	k	(Ar1End)	.	.(Dec)
L	DumpAr2	l	na	CR	
M	ResetE	m	(DispP)	LF	
P	FullReset	p	na		
Q	na	q	(488Cont)		
R	na	r	(ShuntR)		
S	(488Sing)	s	(Send488)		
T	na	t	(TrigLev)		
V	na	v	(MCh2SF)		
W	na	w	(Source)		

The following discussion describes the commands that can be sent over the IEEE 488 interface bus to control the wattmeter. The control is similar to the way the wattmeter is controlled via the

24-button keyboard on the front panel of the wattmeter. Table 8 gives the function of each alphanumeric character sent over the IEEE 488 interface bus. Characters with a function "na" have no affect, those marked in a box have the same affect as the corresponding ones entered from the keyboard, and those with functions in parentheses control the state of the software as described below.

**Table 9** Selection Menu and Default Values

Top of List		
Sample Pulse	Sample Freq.	300 kHz
	Pulse Width	1.00 $\mu$ s
	Conv Cmd Delay	0 ns
	Clock Cor	1097 $\mu$ s/s
Synchronization	Multiplexer	4.68 kHz
	Trigger Level	0.0 V
	Trigger Delay	1 sample
Integration	Hardware Accum.	
	MA Mode	Power
Scale Factor	Shunt Res	1.0
	Ch 1 Scale Factors	(12 Chan 1 SF's)
	Ch 1 Delays	(12 Chan 1 Delays)
	Ch 2 Scale Factors	(12 Chan 2 SF's)
	Ch 2 Delays	(12 Chan 2 Delays)
Display	Display Delay	1000 ms
	Display Ix	(10 Disp Func)
DMA Param	DMA Trigger	TC
	DMA Truncation	None
	DMA Ave	(Blank)
Set Array Lim	Array 1 <b>Beg</b>	0 loc
	Array 1 <b>End</b>	5 loc
	Array 2 <b>Beginning</b>	4096 loc
	Array 2 End	4101 loc
Set 488	Ix=Disp x	(20 Disp Func)
Set State		(See text)

The wattmeter parameters are set by changing the state of the wattmeter and entering the appropriate data for the current state. From the front-panel keyboard the current state can be determined by observing the 32-character display and using the arrow keys to change the state. Table 9 shows the display messages, the sequence of state selections and the default values of the corresponding parameters. Up, Down arrows move from top to bottom in Table 9 and Left, Right arrows move between columns. The list wraps at the top and bottom, i.e., an Up arrow at "Top of List" moves to "Set State" and a Down arrow at "Set State" moves to "Top of List."

The wattmeter state also can be set via the IEEE 488 interface by using the same sequence of commands. The command "E" sets the state to the "Top of List" state. Then, a sequence of arrow commands ("A", "B", "C", or "D") will change the wattmeter state to the desired parameter entry. The parameter value can be changed by entering the proper numeric value or using additional arrow entries, as is appropriate for the specific parameter. A quicker method of changing to some states is to first send the "EA" command, which changes the wattmeter to the "Set State" state. The next character changes the wattmeter to the state given in parentheses in Table 8. As an example, in Table 8, the lower case letter "c" is next to the function MCh1SF, which means to modify the channel 1 scale factors. Thus, to change to the state for modifying the channel 1 scale factors, the command "EAc" is sent.

There are two formats for data transferred from the wattmeter via the IEEE 488 interface. The first format is used for the data dumped from the wattmeter display. These data are sent as a string of 32 characters followed by a CR and LF. Since these data are first written to the display, it can be seen during the transmit process. The second format is used for the hex data from the two DMA arrays. These data are sent as a string of 29 characters followed by a CR and LF. Each of these strings contains the data for six array locations. Each location is represented as four hex characters followed by a space. The hex code used is 0 to 9 for the first 10 numbers and :, ;, <, =, >, and ? for A, B, C, D, E, and F respectively.

The wattmeter originally was controlled by an 8086 microprocessor on an Intel SDK-86 computer board. As part of the upgrade to add the IEEE 488 interface to the wattmeter, the control was changed to an Intel 86/12A Multibus microcomputer, which also contains an 8086 microprocessor. This change required the re-addressing of the programmable peripheral interface (PPI) device and the interrupt handler device.

## 4.2. Software Changes for HASW Upgrade

The software upgrade for the changes to convert the Wideband Sampling Wattmeter to the HASW involved the differences with the new multiplier-accumulator board. The multiplier-accumulator, (MA) mode setting is accommodated as is the reading of the larger hardware accumulator, 47 bits vs 35 bits. Also, the allocation of time between the number of hardware accumulations and the number of software accumulations is changed. Depending on the MA mode, the wattmeter calculates and displays the input power, the average of the channel 1 inputs, the average of the



channel 2 inputs, or the ratio of the number of samples counted by the frequency control and programmable time delay board and the number of samples counted by the multiplier-accumulator board. This last measurement should always be the numerical value 1 for a properly operating wattmeter.

## 5. Performance

The critical factors that are of interest for the performance of the HASW are the noise level, frequency response, and temperature coefficients of the input circuitry. The noise levels of the input circuitry were measured by applying a constant dc signal or a short circuit to the voltage- and current-input modules and then recording the range of digital codes generated by the modules. The final design achieved an approximate noise level of plus/minus one code width. The data shows about 60 percent of the output at one code, 15 percent to 25 percent at each of the adjacent codes, and 1 to 2 percent at plus and minus two codes. Figure 2 shows a typical distribution of codes for 100 samples of the voltage-input module with the input terminal shorted. Similar results are observed for the current-input module.

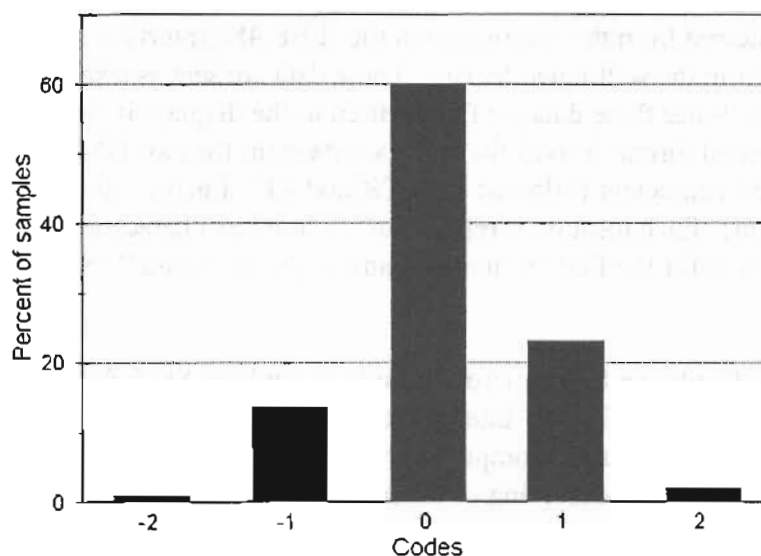


**Figure 2** Typical Distribution of Voltage Codes for Shorted Input.

The frequency response of the two input modules was determined using sine waves from a standard commercial calibrator, and using an ac/dc thermal voltage-converter comparator to measure the amplitude of the test signals. Figure 3 shows the frequency response of the current-input module and Figure 4 shows the frequency response of the voltage-input module. The frequency response of the 255 V range is marginal for achieving the project goal of an uncertainty less than  $\pm 50 \mu\text{W/W}$  of full scale. Attempts will be made to reduce the errors for this input range

by redesigning the attenuator for this range. The other ranges have errors that are well within the uncertainty goal.

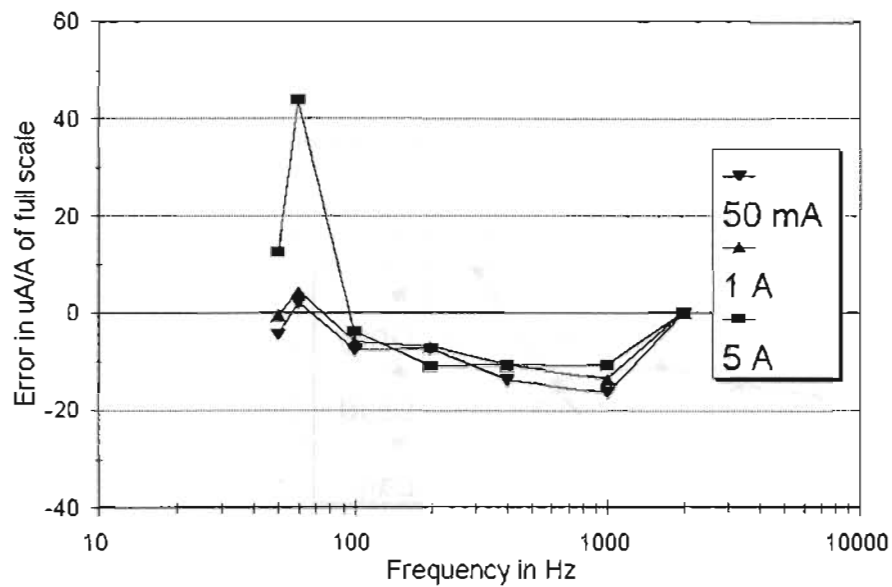


Figure 3 Frequency Response of Current-Input Module.

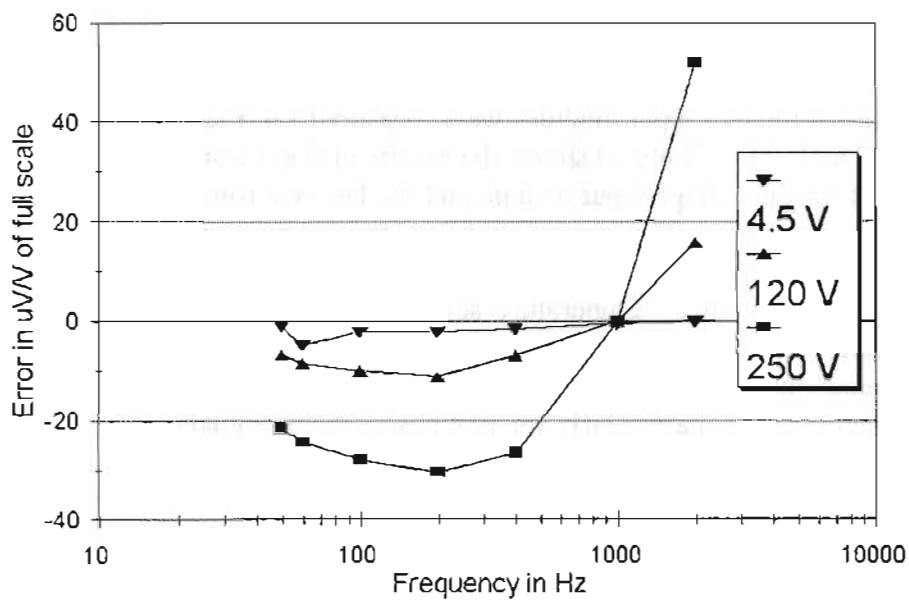
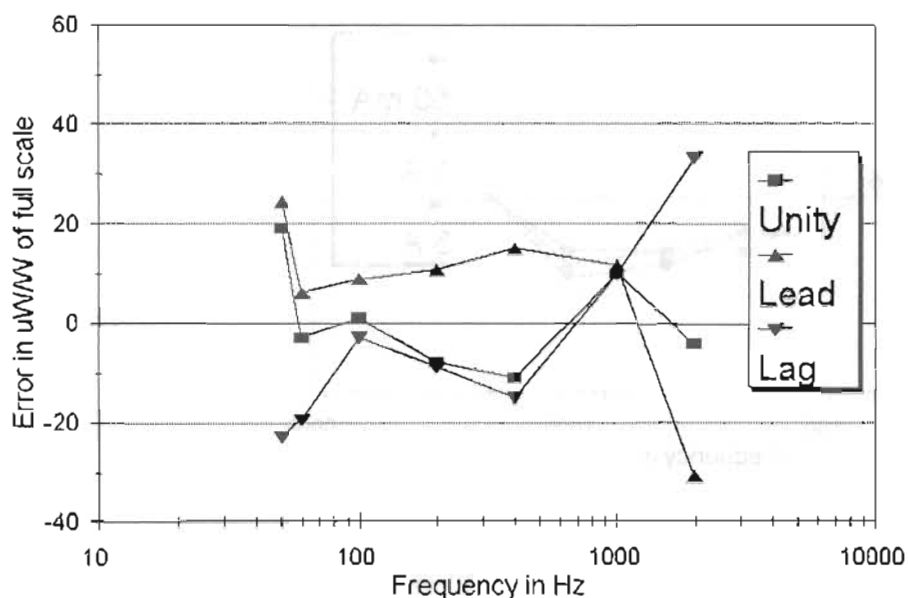


Figure 4 Frequency Response of Voltage-Input Module.

The power frequency response was measured using the NIST Audio-Frequency Power Bridge [3]. Figure 5 shows the typical results for calibration of the HASW for power measurements. This graph shows the power errors for unity and zero power-factor lead and lag signals with voltage and current amplitudes of 120 V and 1 A. These results show that the power uncertainty goal of less than  $\pm 50 \mu\text{W/W}$  of full scale range was achieved.



**Figure 5** Frequency Response of Power Measurements.

The temperature sensitivities of the two input modules were measured for a temperature change of about 25 °C, from 10 °C to 35 °C. Table 10 shows the results of these tests. The first three rows are the results obtained for the voltage-input module and the last two rows show the results obtained for the current-input module. The temperature sensitivities range up to 2.6 parts in  $10^6/^\circ\text{C}$  for the voltage-input module and up to 3.6 parts in  $10^6/^\circ\text{C}$  for the current-input module. Based on these data, the expected power temperature sensitivity is about 5 parts in  $10^6/^\circ\text{C}$ . However, each of the module sensitivities were measured independently, so no information was obtained to determine the temperature sensitivity of the phase of each module. Thus, the power sensitivity may be significantly larger, particularly for low power-factor signals.



Table 13 Temperature Sensitivities for the Input Modules in parts in  $10^6/^{\circ}\text{C}$

Range	50 Hz	400 Hz	1 kHz
3 V	0.9	2.6	2.6
120 V	2.1	2.3	-1.3
240 V	0.4	1.1	1.6
1 A	2.5	2.5	2.9
5 A	3.6	3.2	2.9

## Acknowledgments

The authors gratefully acknowledge the assistance of T. Michael Souders with the design of the two-stage current-transformer, the help of Owen B. Laug with the design of the input circuitry, the aid of Nile M. Oldham in solving several calibration problems, the assistance of Bryan C. Waltrip and Mark Parker with performing power calibrations, the help of Robert Palm in preparing the drawings and the editorial support and review provided by Barry A. Bell.

## References

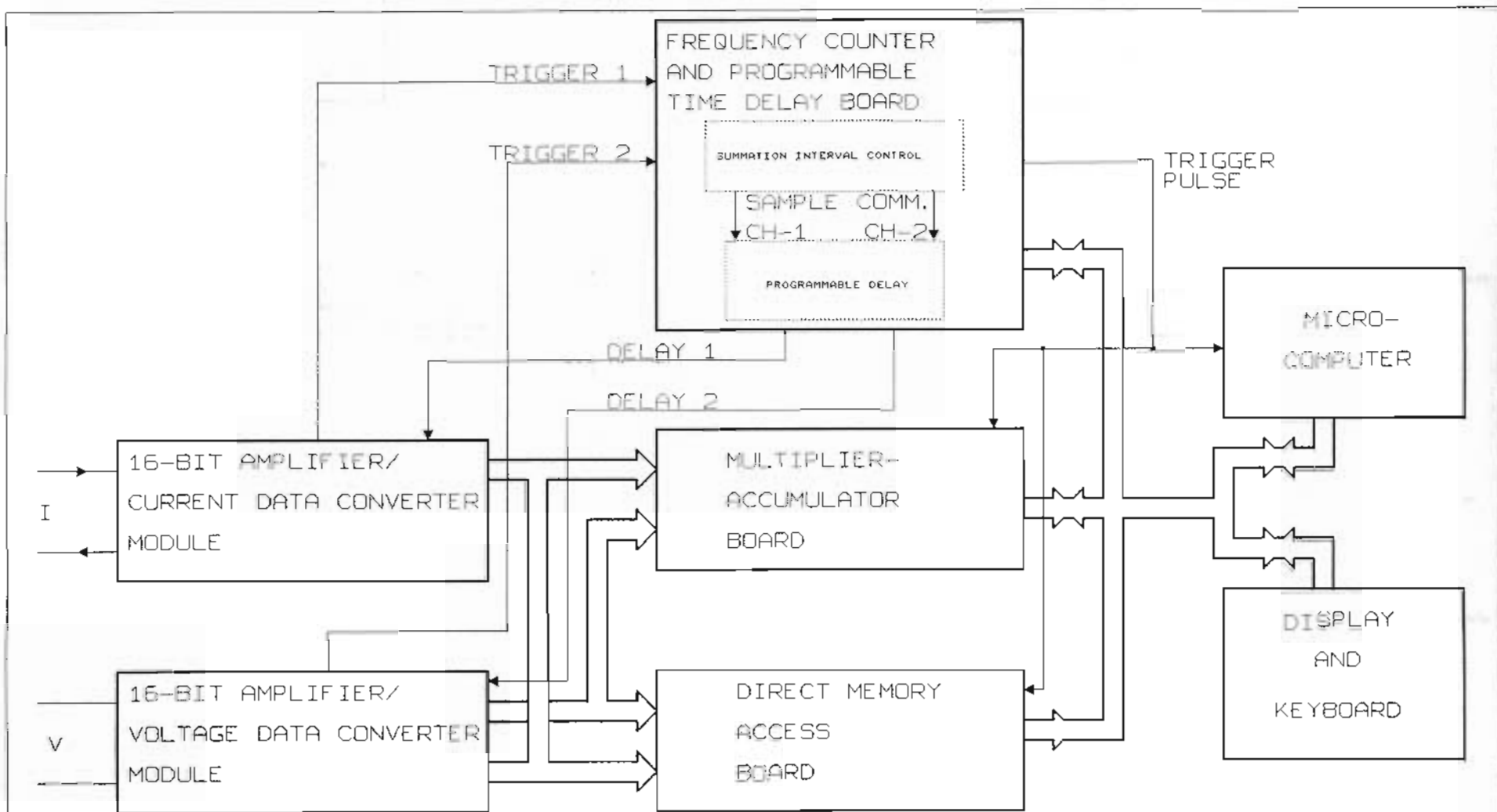
- [1] G.N. Stenbakken, "A Wideband Sampling Wattmeter," *IEEE Trans. Power Appar. Syst.*, PAS-103, pp. 2919-2926, Oct. 1984.
- [2] G.N. Stenbakken, O.B. Laug, T.H. Kibalo, B.A. Bell, and A.G. Perrey, "NBS Wideband Sampling Wattmeter," NBS Technical Note 1221, (U.S. Government Printing Office, Washington, DC, May 1987).
- [3] B.C. Waltrip and N.M. Oldham, "Performance Evaluation of a New Audio-Frequency Power Bridge," *IEEE Trans. Instrum. Meas.*, IM-40, pp. 380-383, Apr. 1991.
- [4] R.S. Turgel, "Digital Wattmeter Using a Sampling Method," *IEEE Trans. Instrum. Meas.*, IM-23, Dec. 1974.
- [5] M.F. Matouka, "A Wide-Range Digital, Power/Energy Meter for Systems With Nonsinusoidal Waveforms," *IEEE Trans. on Industrial Electronics*, IE-29, pp. 18-31, Feb. 1982.
- [6] J.J. Hill and W.E. Alderson, "Design of a Microprocessor-Based Digital Wattmeter," *IEEE Trans. on Industrial Electronics and Control Instrumentation*, IECI-28, Aug. 1981.
- [7] F.J.J. Clark and J.R. Stockton, "Principles and Theory of Wattmeters Operating on the Basis of Regularly Spaced Sample Pairs," *Jour. of Physics E: Scientific Instruments*, Vol. 15, No. 6, pp. 645-652, June 1982.
- [8] T.M. Souders, "A Wide Range Two-Stage Current Transformer of High Accuracy," *IEEE Trans. Instrum. Meas.*, IM-21, pp. 340-345, Nov. 1972.

## Appendix - Drawings

The following drawings show the parts of the wattmeter that were changed during the upgrade from the NIST Wideband Sampling Wattmeter to the NIST High-Accuracy Sampling Wattmeter.

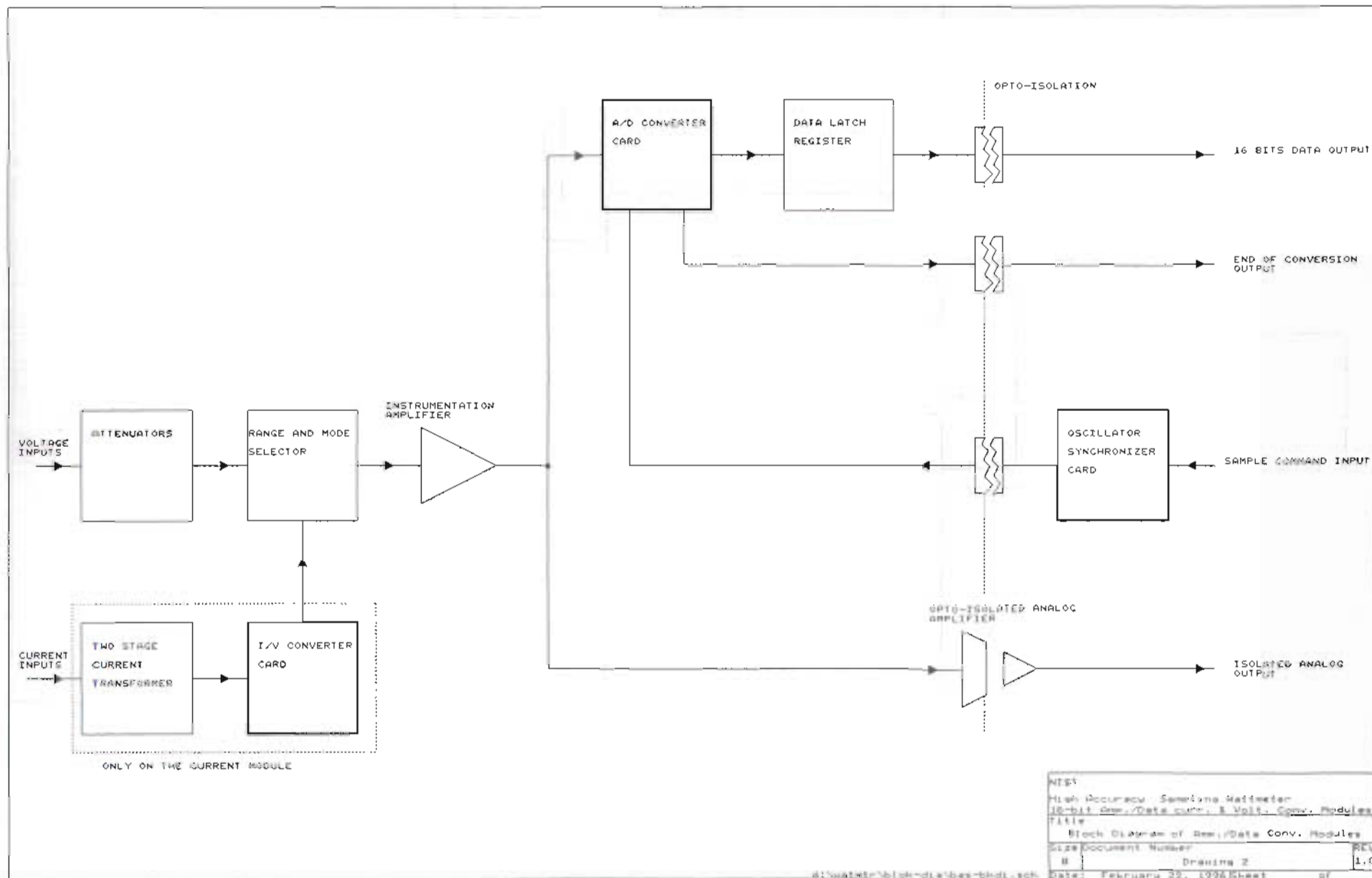
Drawing 1	Basic Block Diagram of HASW	A1
Drawing 2	Basic Block Diagram of Converter Modules	A2
Drawing 3	Block Diagram of Amp/Data Converter Modules	A3
Drawing 4	Block Diagram & Power Supply	A4
Drawing 5	Clock-Synchronizer Board	A5
Drawing 6	ADC Board 1 (Analogic)	A6
Drawing 7	ADC Board 2 (Crystal)	A7
Drawing 8	16-bit Amp/Data Curr. & Volt Conv Modules, Mother Board	A8
Drawing 9	Current Transformer Schematic	A9
Drawing 10	Current-to-Voltage Converter Board	A10
Drawing 11	Multiplier-Accumulator - Block Diagram 1	A11
Drawing 12	Multiplier-Accumulator - Block Diagram 2	A12
Drawing 13	16-bit Mult-Acc Board - Part A and Part B	A13
Drawing 14	16-bit Mult Acc Board - Board Layout Schematic	A14
Drawing 15	Sequencer Timing Diagram	A15
Drawing 16	End-of-Conversion Combiner Circuit	A16
Drawing 17	Ground Connection Schematic	A17
Drawing 18	System Power Supply Block Diagram	A18
Drawing 19	Time Delay Extension	A19
Drawing 20	Frequency Counter and Programmable Time Delay Board	A20





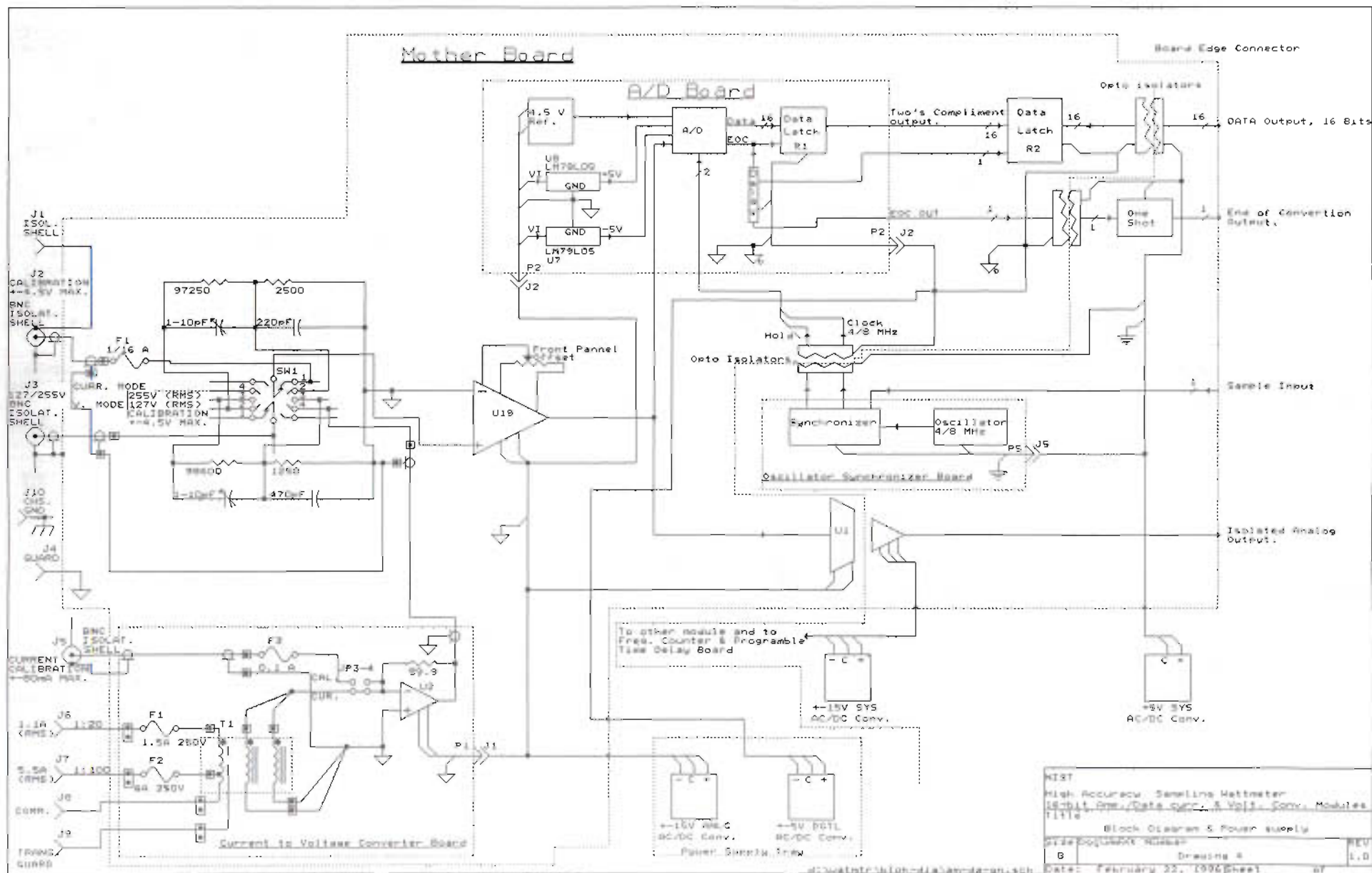
d:\metr\belokndia\um-gb1kd.sch

MST		
MST Accuracy Sampling Matrices		
Title Basic Block Diagram of Measurement System		
Size	Document Number	REV
6	Drawing 1	1.0
Date:	May 2, 1996	Sheet 1 of 1



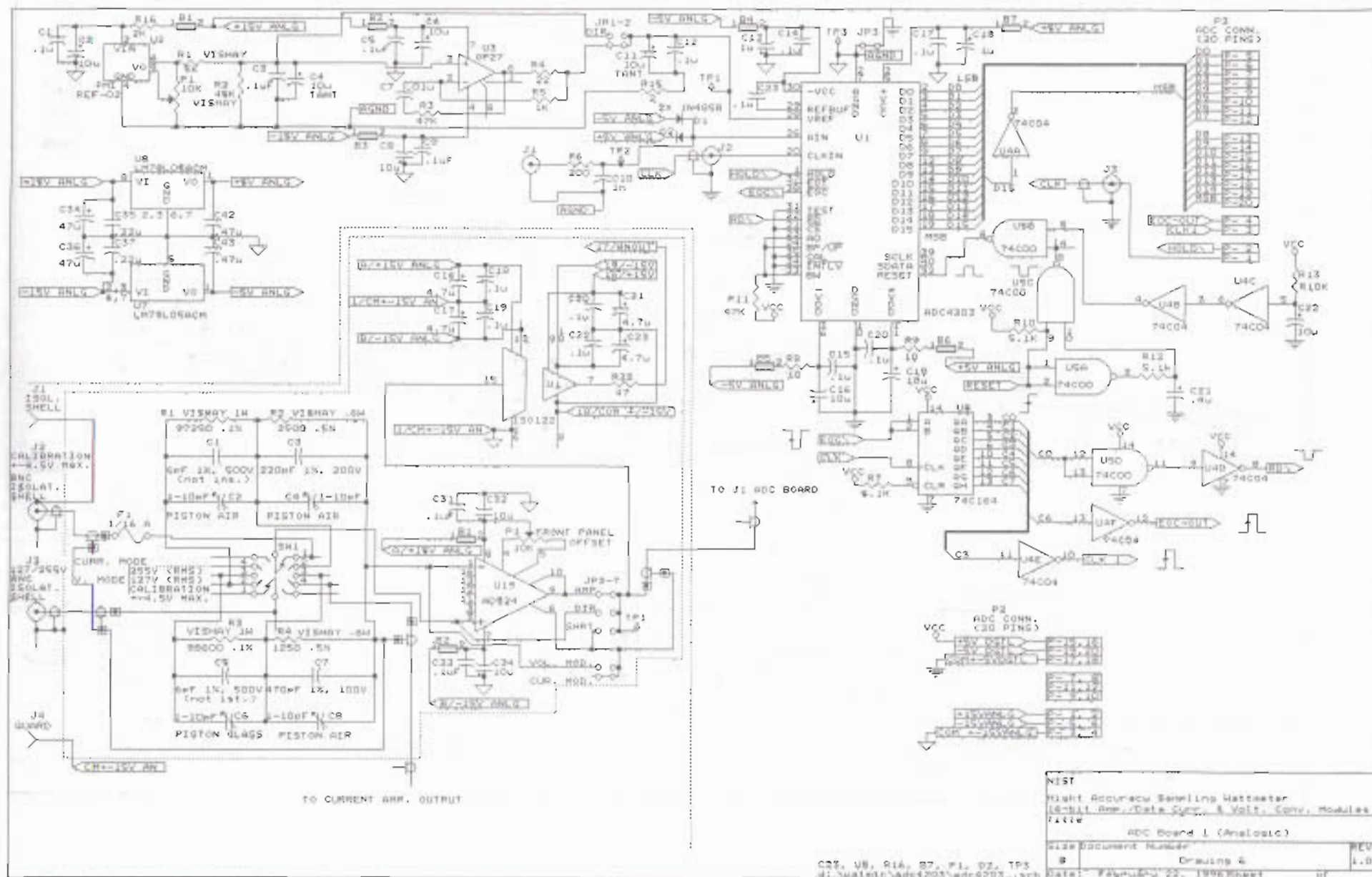
NIST		
High Accuracy Sampling Multimeter		
16-bit Conv./Data conv. & Volt. Conv. Modules		
Title		
Block Diagram of Rev./Data Conv. Modules		
Size/Document Number		
B	Drawing 2	REV 1.0
Date: February 29, 1996 Sheet 1 of 1		











NIST

Flight Accuracy Sensing Wattmeter  
16-bit Anal./Data Conv. & Volt. Conv. Modules  
Title

ADC Board 1 (AnalogIC)

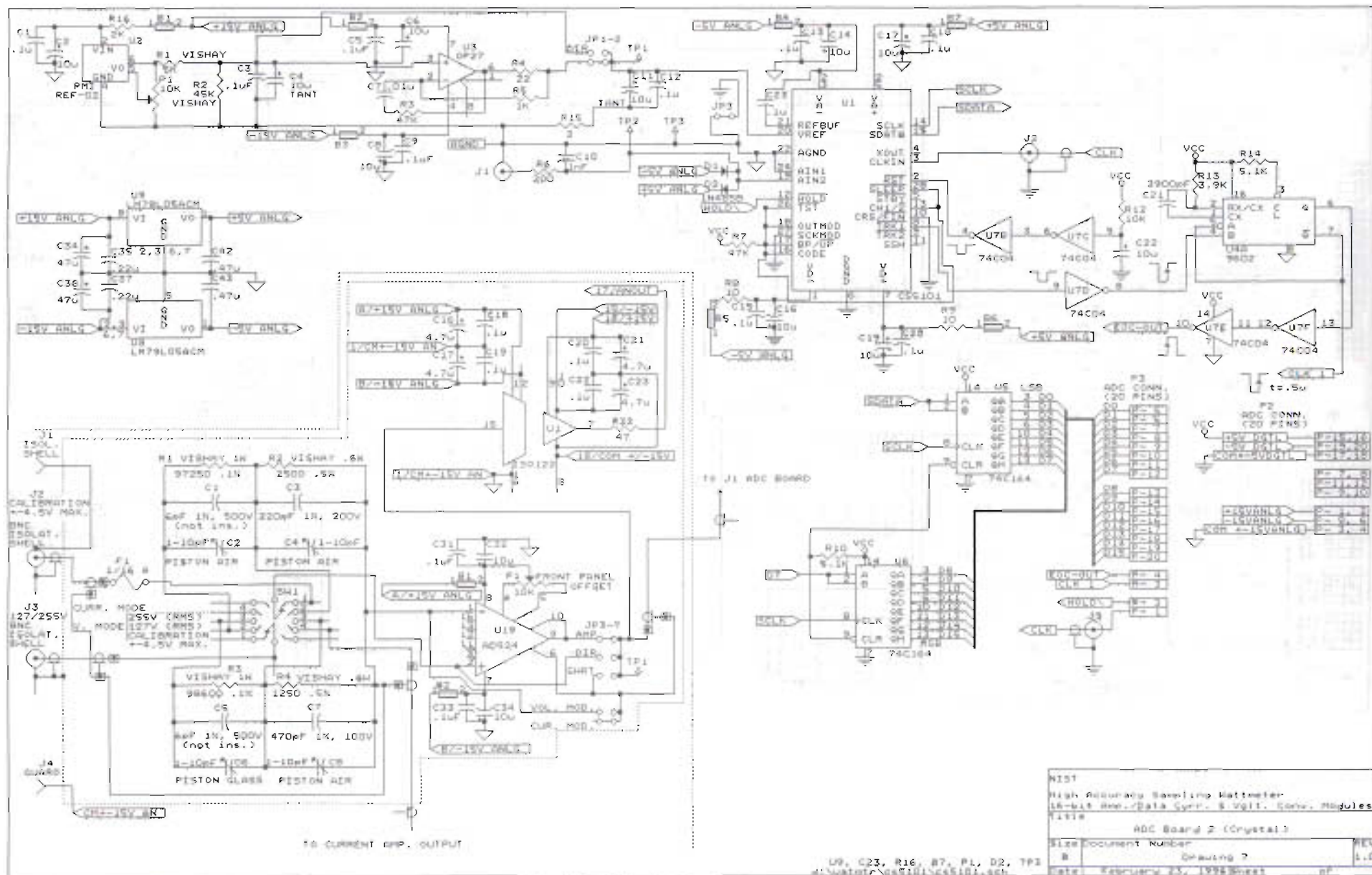
size Document Number

1

Downloaded At: 11:53 11 September 2009

REV  
A-9

Class	February 22, 1995
-------	-------------------



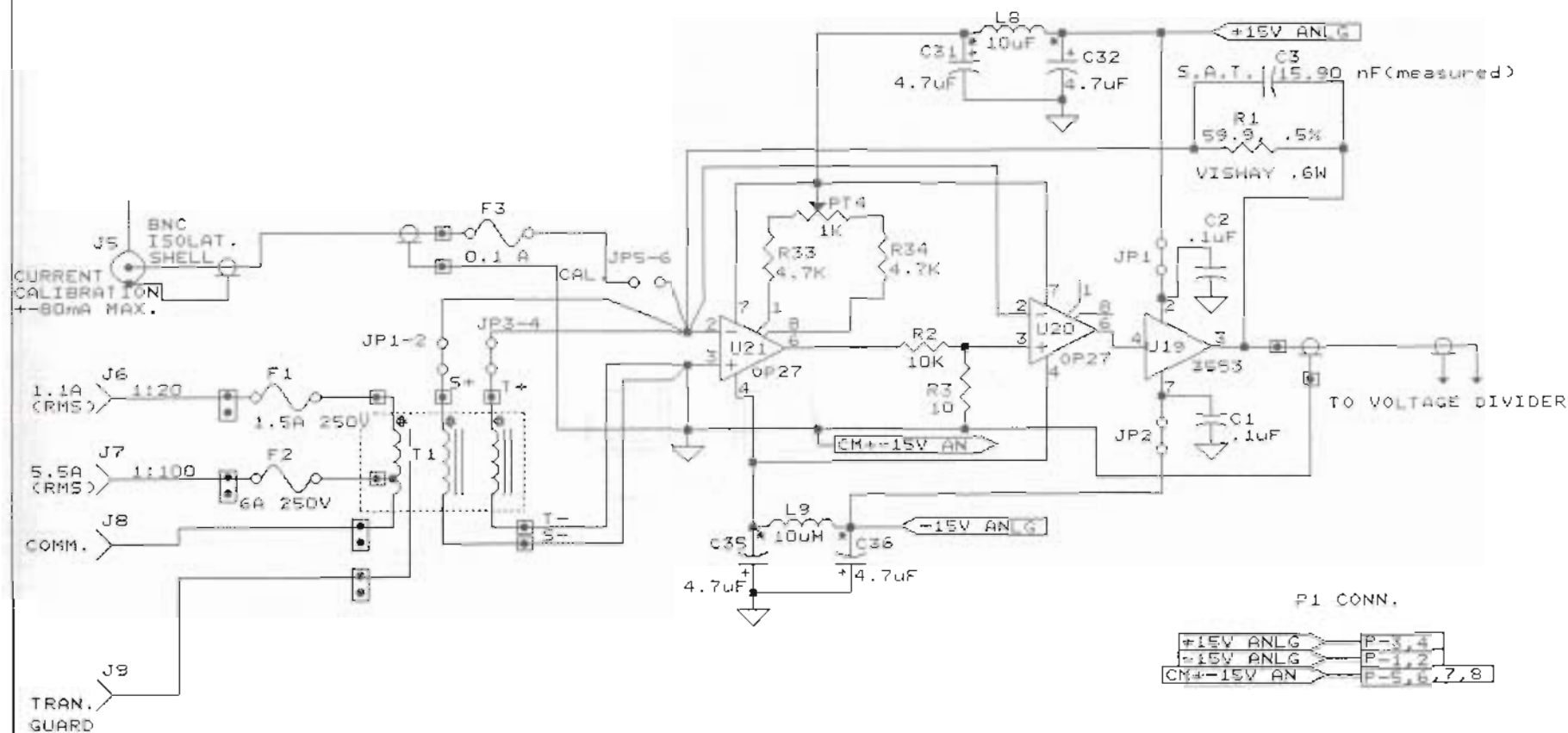
NIST		
High Accuracy Sampling Meter		
16-bit Anal. Data Conv. & Volt. Conv. Modules		
Title		
ADC Board 2 (Crystal)		
Size	Document Number	REV
B	Drawing 1	1.0
Date	February 23, 1998	of

Diagram illustrating the construction schematic of the magnetic shield. It shows two cores, CORE #1 and CORE #2, positioned horizontally. CORE #1 is on the left, and CORE #2 is on the right. The shield is divided into two horizontal sections: the UPPER HALF OF MAGNETIC SHIELD (top) and the LOWER HALF OF MAGNETIC SHIELD (bottom). The cores are connected by a central vertical section.

Freq. (Hz)	$I_p$ (A)	$V_o$ (V)	$Z_{in}$ ( $\Omega$ )
50	0.04	1.8	450
1K	0.0206	5.13	2490
10K	0.0034	11.8	12K

Freq. (Hz)	$I_p$ (A)	$V_o$ (V)	$Z_{m2}$ ( $\Omega$ )
50	0.0385	1.67	433
1K	0.017	5.2	2470
10K	0.0094	11.31	12.5K

NIST  
 High Accuracy Sampling Wattmeter  
 15-bit Anal/Dig, Current Conv. Module  
 Title: Current transformer schematic  
 Size: Document Number: REV  
 8 Drawing 8 1.0  
 Date: February 23, 1996 Sheet of



NIST

High Accuracy Sampling Wattmeter  
16-bit Amplifier/Data Curr. Converter Module  
Title

Current-to-Voltage Converter Board

Size Document Number

A

Drawing 10

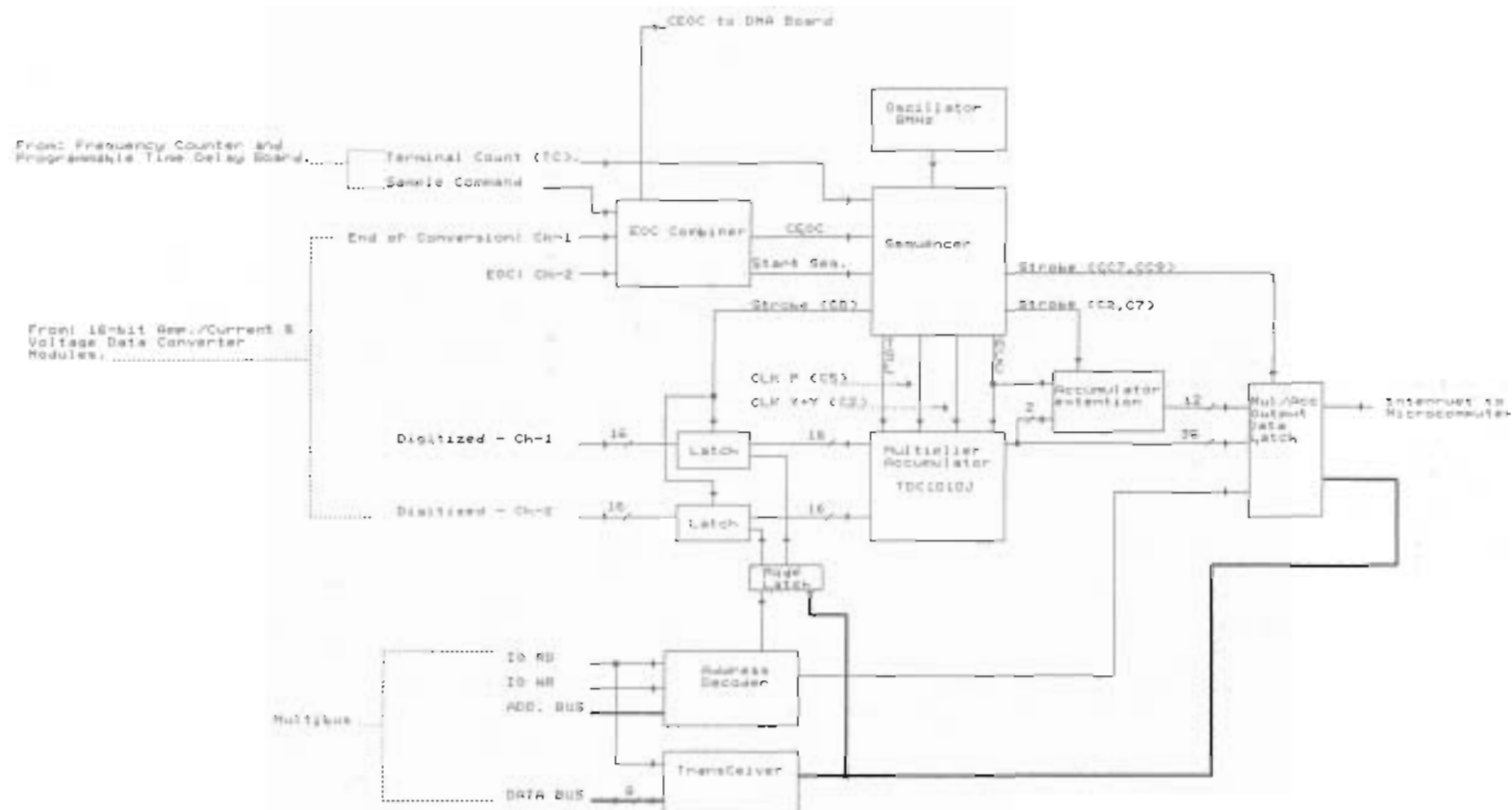
REV

1.0

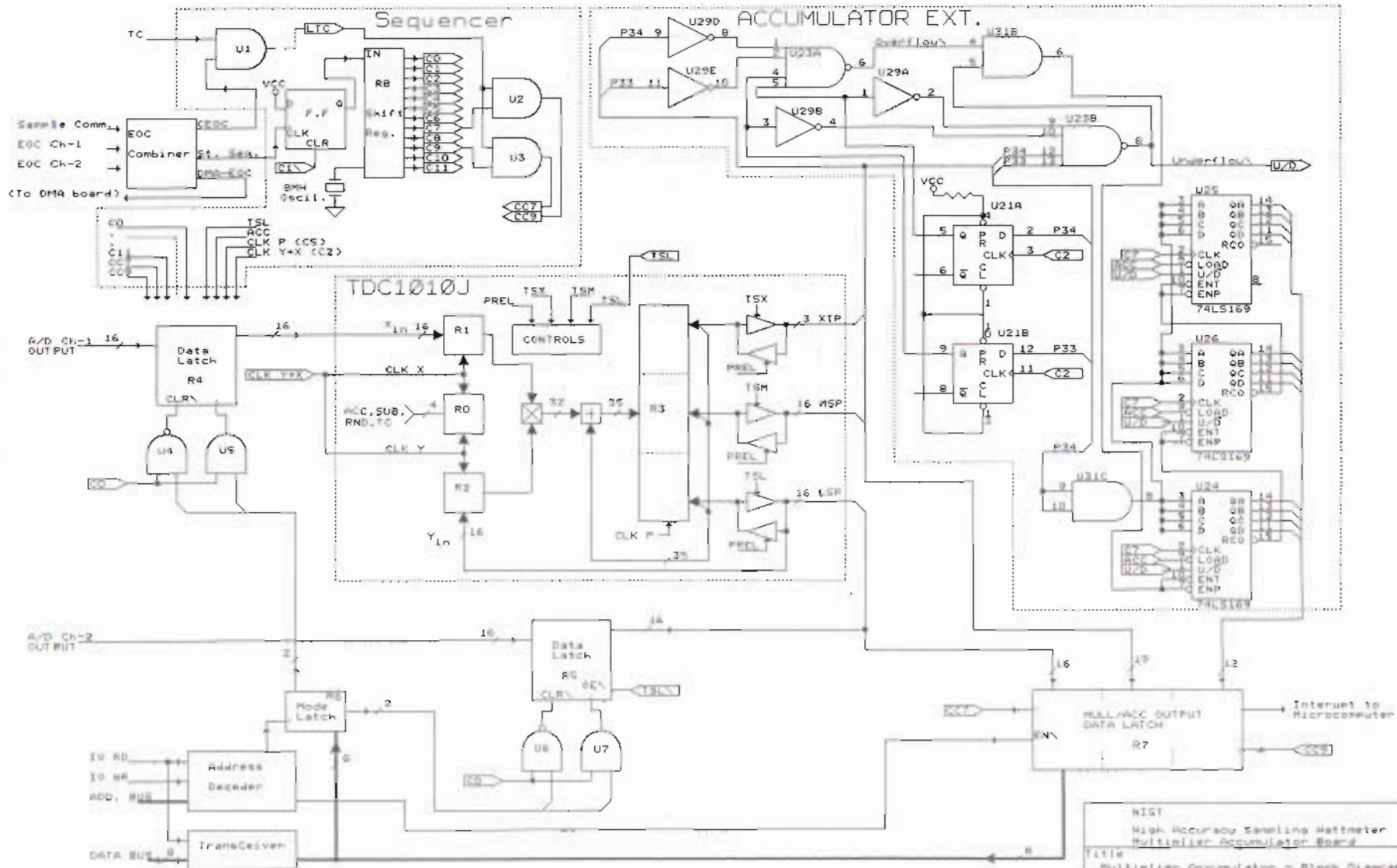
Date: February 23, 1996 Sheet of

d:\watmtr\in-mod2\1-conv2.sch

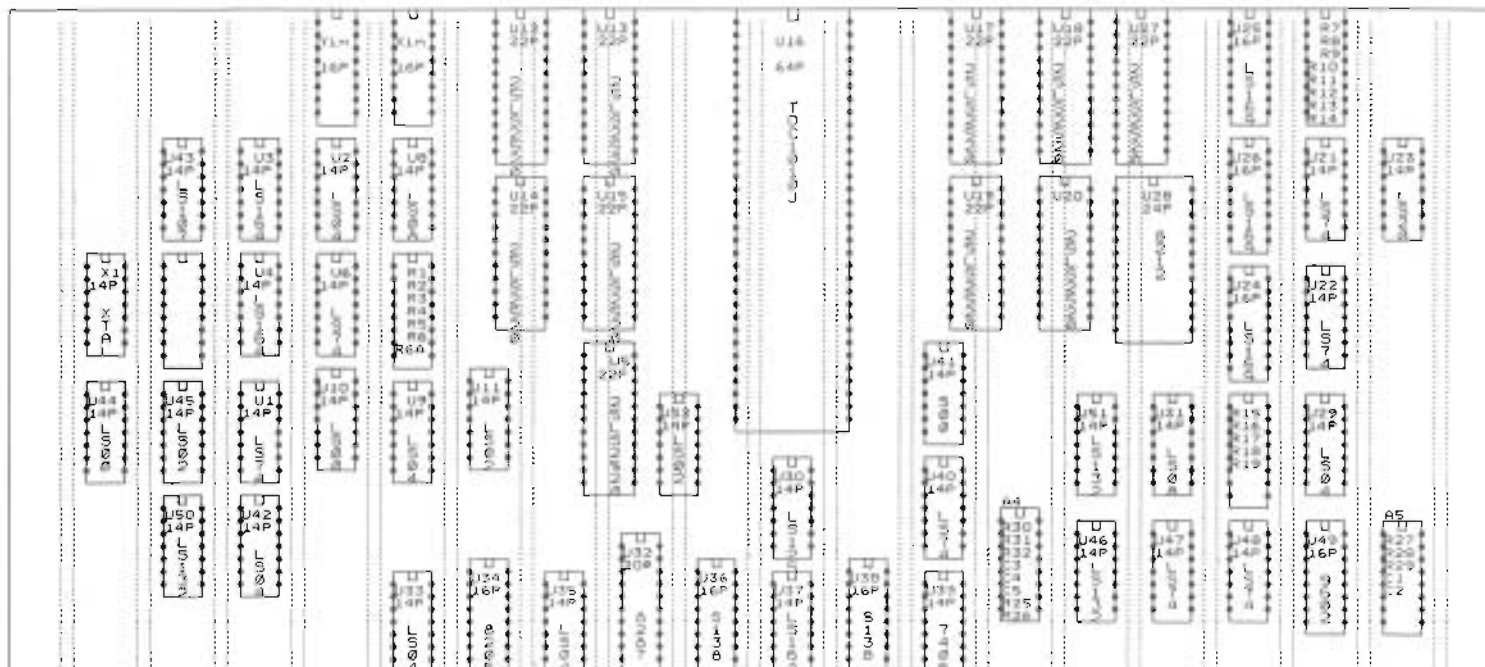




8157		
High Accuracy Sampling Multimeter		
Multiplier Accumulator Board		
Title		
Multiplier Accumulator - Block Diagram 1		
Size Document Number		
8	Drawing 11	REV
		1.0
Date: February 23, 1996		
Sheet 1 of 1		

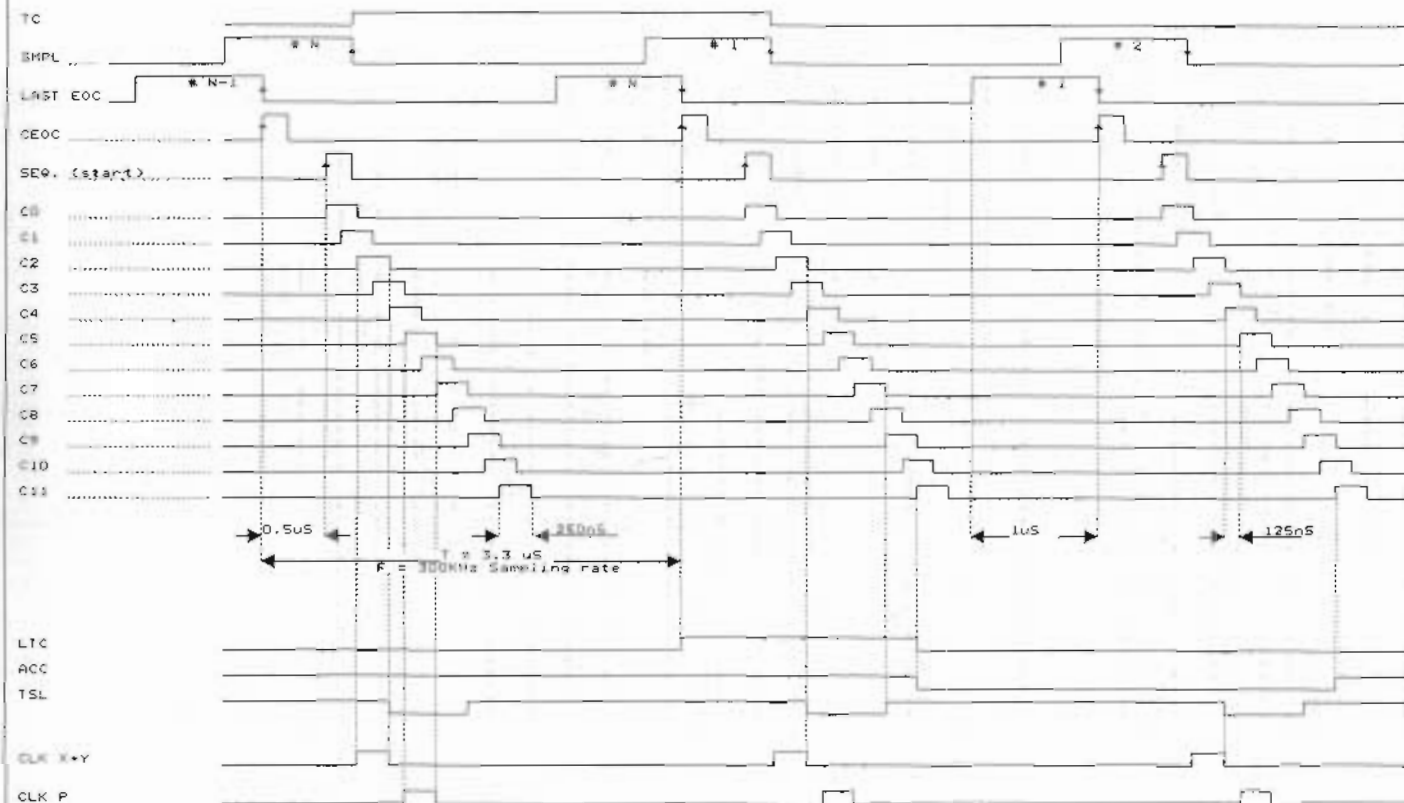


H151  
 High Accuracy Sampling Wattmeter  
 Multplier Accumulator Board  
 Title  
 Multplier Accumulator - Block Diagram 2  
 Size Document Number  
 B Drawing 12  
 Date: February 21, 1978 Rhesi

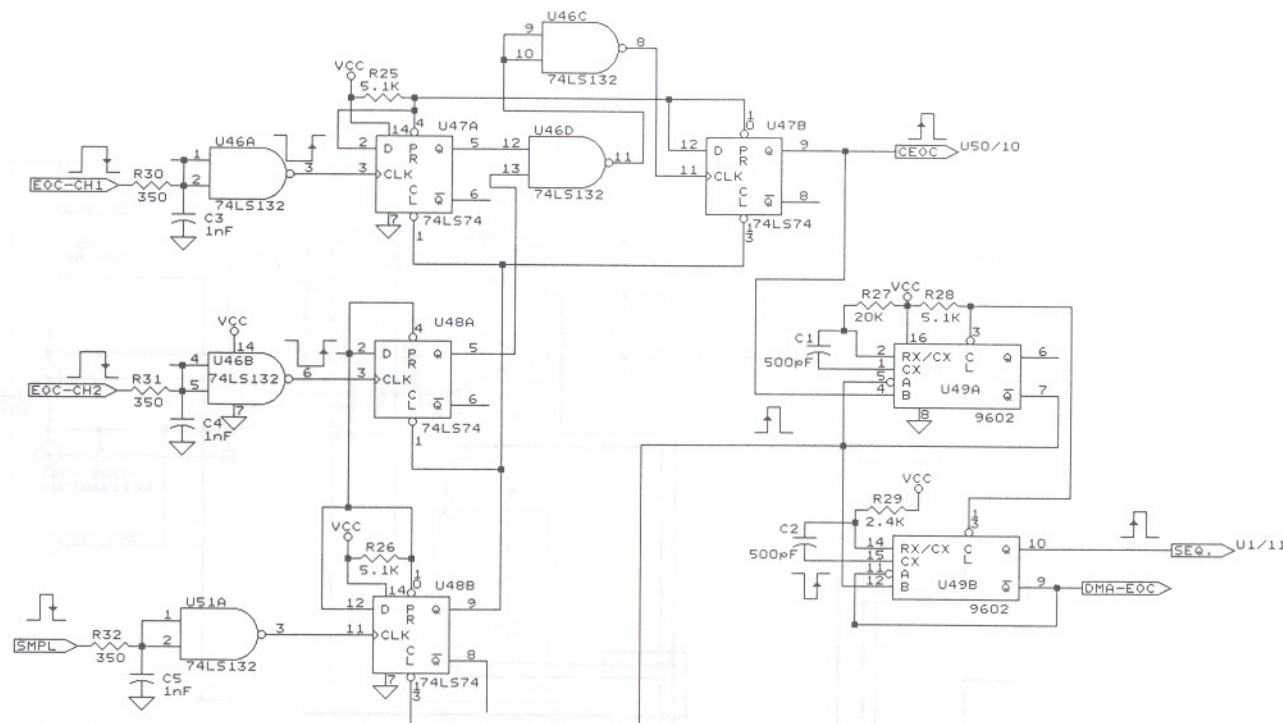


NIST		
High Accuracy Sampling Wattmeter		
16-bit Multiplier Accumulator Board		
Title		
Board Layout Schematic		
Size Document Number		
8	Drawing 14	REV
Date	February 21, 1998	Sheet 2

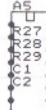
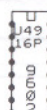
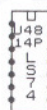
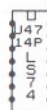
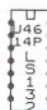
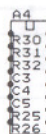
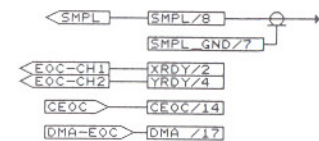
US2, R33, CS  
41/ualetc/oul-acc/ma-64.drv



NIST		
High Accuracy Sampling Multimeter		
16-bit Multisample Accumulator Based		
Sequencer Block		
File		
Sequencer Timing Diagram		
Size Document Number		
B	Drawings IS	REV
Date: February 23, 1995		1.0



60 PIN CONN.  
P3



A4

R30 100  
R31 100  
R32 100  
C3 1nF  
C4 1nF  
C5 1nF  
R25 5.1K  
R26 5.1K

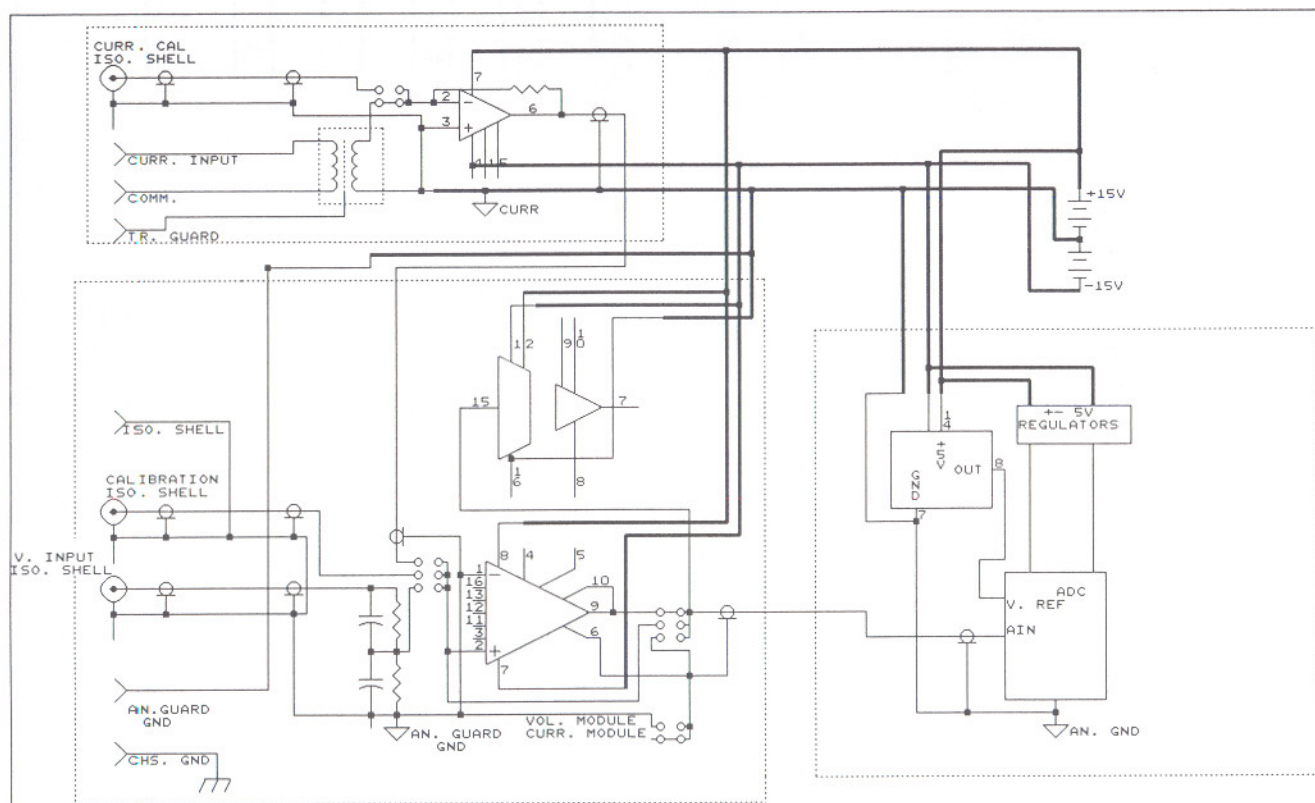
A5

R27 2.4K  
R28 5.1K  
R29 2.4K  
C1 500pF  
C2 500pF

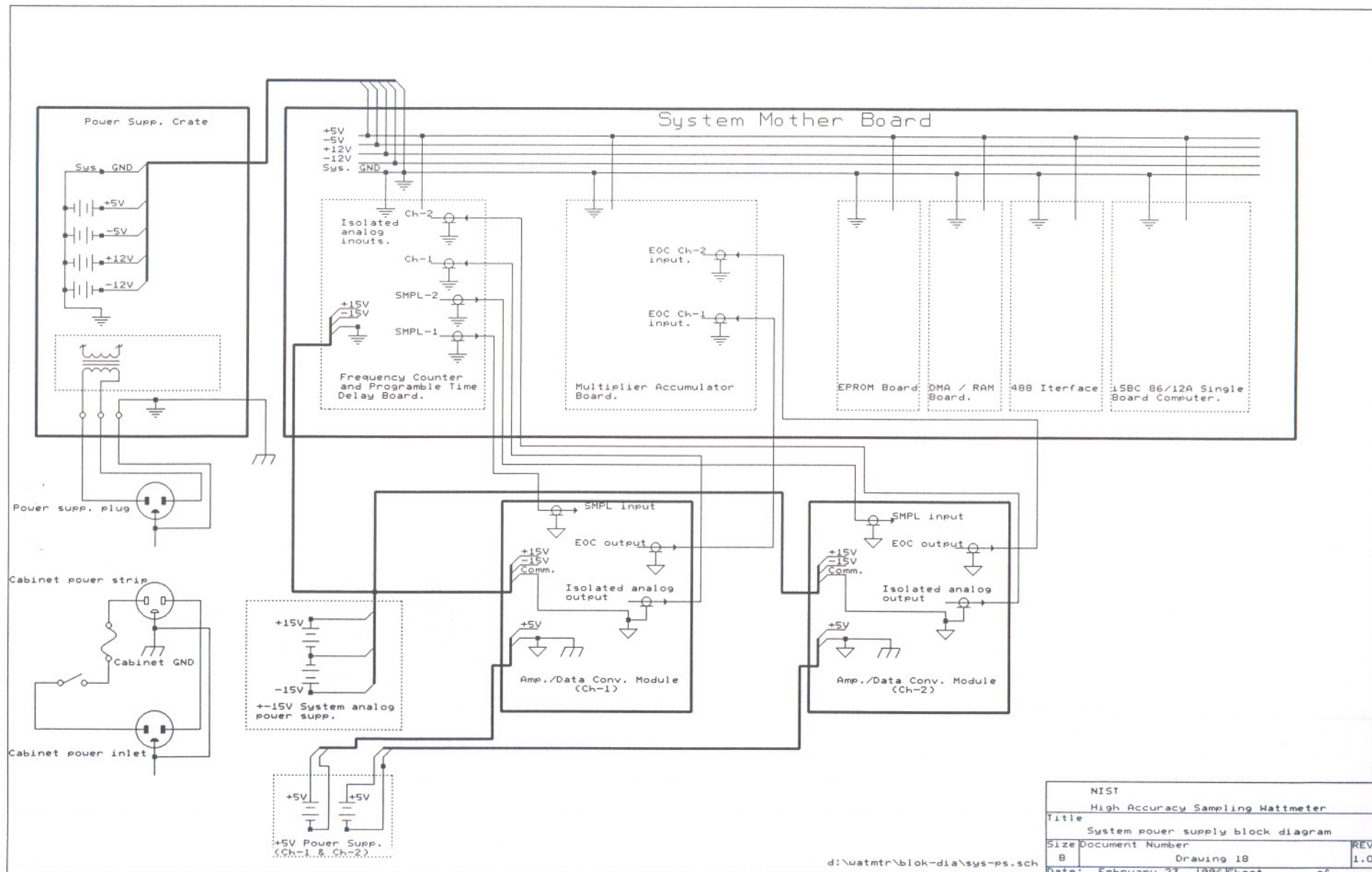
NIST		
High Accuracy Sampling Wattmeter		
16-bit Multiplier Accumulator Board - Part B		
Title		
End-of-Conversion Combiner Circuit		
Size	Document Number	REV
B	Drawing 16	1.0
Date:	February 23, 1996	Sheet of

R32, U51, C5, A5,  
D:\watmtr\mul-acc\ceoc.sch





NIST		
High Accuracy Sampling Wattmeter		
16-bit Amp./Data Curr. & Volt. Conv. Modules		
Title		
Ground Connection Schematic		
Size	Document Number	REV
B	Drawing 17	1.0
Date:	February 23, 1996	Sheet of



NIST			
High Accuracy Sampling Wattmeter			
Title			
System power supply block diagram			
Size	Document Number	REV	
B	Drawing 18	1.0	
Date: February 23, 1996		Sheet	of

d:\watmtr\blok-dia\sys-ps.sch